Coherence of Bangui Magnetic Anomaly with Topographic and Gravity Contrasts across Central African Republic

Polina Lemenkova, Olivier Debeir

minerals

MDPI

Article

Coherence of Bangui Magnetic Anomaly with Topographic and Gravity Contrasts across Central African Republic

Polina Lemenkova * and Olivier Debeir

Laboratory of Image Synthesis and Analysis (LISA), École Polytechnique de Bruxelles (Brussels Faculty of Engineering), Université Libre de Bruxelles (ULB), Campus du Solbosch, Building L, ULB—LISA CP165/57, Avenue Franklin D. Roosevelt 50, 1050 Brussels, Belgium; olivier.debeir@ulb.be

* Correspondence: polina.lemenkova@ulb.be; Tel.: +32-471-86-04-59

Abstract: The interactions between the geophysical processes and geodynamics of the lithosphere play a crucial role in the geologic structure of the Earth's crust. The Bangui magnetic anomaly is a notable feature in the lithospheric structure of the Central African Republic (CAR) resulting from a complex tectonic evolution. This study reports on the coherence in the geophysical data and magnetic anomaly field analysed from a series of maps. The data used here include raster grids on free-air altimetric gravity, magnetic EMAG2 maps, geoid EGM2008 model and topographic SRTM/ETOPO1 relief. The data were processed to analyse the correspondence between the geophysical and geologic setting in the CAR region. Histogram equalization of the topographic grids was implemented by partition of the raster grids into equal-area patches of data ranged by the segments with relative highs and lows of the relief. The original data were compared with the equalized, normalized and quadratic models. The scripts used for cartographic data processing are presented and commented. The consistency and equalization of topography, gravity and geoid data were based using GMT modules 'grdfft' and 'grdhisteq' modules. Using GMT scripts for mapping the geophysical and gravity data over CAR shows an advanced approach to multi-source data visualization to reveal the relationships in the geophysical and topographic processes in central Africa. The results highlighted the correlation between the distribution of rocks with high magnetism in the central part of the Bangui anomaly, and distribution of granites, greenstone belts, and metamorphosed basalts as rock exposure. The correspondence between the negative Bouguer anomaly (<−80 mGal), low geoid values (<−12 m) and the extent of the magnetic anomaly with extreme negative values ranging from −1000 to −200 nT is identified. The integration of the multi-source data provides new insights into the analysis of crustal thicknesses and the average density of the Earth in CAR, as well as the magnitude of the magnetic fields with notable deviations caused by the magnetic flux density in the Bangui area related to the distribution of mineral resources in CAR.

Keywords: programming; geophysics; GMT; mapping; Africa; geology; geodynamics; geomatics; data analysis; cartography

Citation: Lemenkova, P.; Debeir, O. Coherence of Bangui Magnetic Anomaly with Topographic and Gravity Contrasts across Central African Republic . *Minerals* **2023**, *13*, 604. https://doi.org/10.3390/min13050604

Academic Editors: Gianluca Bianchini, Claudio Natali, Chiara Marchina and Valentina Brombin

Received: 22 February 2023
Revised: 23 April 2023
Accepted: 24 April 2023
Published: 27 April 2023

1. Introduction

1.1. Background

The problem of feature matching in Earth studies can be described as matching the extent, direction and intensity of the geophysical and geologic processes, objects and phenomena visualised on the maps. A particular geophysical orgeologic feature is associated with a coordinate position in a cartographic domain identifying its location, and variables representing its appearance either by the points for discrete objects or by the fields for continuum processes. For analysis of correlation and links between diverse geologic and geophysical variables, matched feature points and continued fields represented on the maps should maintain similar regional appearance as well as relative spatial relationships with other processes, e.g., variation in topography or geoid and regional distribution of

the geologic units. Analysis of correlation between geophysical and geological variables has extensive uses in integrated geophysical and seismic analysis [1], hydrological and engineering geological studies [2–4], geophysical anomalies [5], mineral exploration [6], or landslide hazard risk assessment in the areas with complex geology [7,8].

Each cartographic-matching method supports either a specific data format, e.g., such as ArcGIS shape files [9–11] or the tiled format for image processing in remote sensing software [12,13] or a limited set of converted and imported data formats from the multi-source data [14–16]. Scripting and programming methods also showed their effectiveness in matching tasks and coherence analysis when dealing with topographic and geophysical datasets since they optimise the workflow via smooth, automated and rapid approaches in data processing. For instance, scripts facilitate the modelling of geochemical–geophysical inversion to investigate the issues of dynamic topography [17], enable automated and optimised isolines approximation and mesh gradation in topographic data processing [18], or support detailed topographic analysis through 3D cross-sections [19,20].

1.2. Hypothesis and Research Questions

The effects of the geophysical and geological factors on each other have not been well observed in a more structural manner in the existing literature. In response to this, a conceptual framework for this study was developed based on a set of hypotheses derived from the literature review and considering the local context of CAR. We proposed a hypothesis as follows: the Bangui magnetic anomaly is strongly associated with the regional geophysical and geologic setting in CAR. As such, we focus on the following questions in this study:

- (Q1): Is the Bangui magnetic anomaly positively associated with geophysical and topographic settings in the CAR, gravity values and free-air anomaly?
- (Q2): Is the Bangui magnetic anomaly associated with the distribution of the geologic setting in the region?

To answer these question and test the hypothesis, we address the problem of the unified cartographic matching framework that supports a large family of data formats technically implemented in the Generic Mapping Tools (GMT) and QGIS. Our goal is to present a scripting cartographic approach that exploits the structural regularities in the geophysical, geologic and topographic datasets on the Central African Republic (CAR) and uses them as input information during matching procedure. In this regard, this study aims at presenting a cartographic interpretation of the Bangui magnetic anomaly and an analysis of its consistence using the available data on geophysical and geological settings of the CAR. Technically, we optimised the operational workflow of the cartographic work through the use of scripts.

To this end, we introduced a scripting cartographic framework that uses Bash scripts and GMT commands for automation of the cartographic workflow. We first extract all the information from the gravity, topography and magnetic grids and map their parameters. Afterwards, we detect and separately analyse the repeated structures in the topographic grids. This is done using equalisation and comparison of the equalised, quadratic, normalized and original rasters through enhanced ranges of a grid depending on frequency distribution of elevation amplitude of the relief in various regions of the CAR. The raster images were independently incorporated and processed as separate files. The scripts used for implementation of the cartographic work are presented in the Appendix A with added comments on the most essential details of the GMT codes presented in the Methodology section.

Moreover, the coherency between the vertical gradient and the distribution of gravity anomalies is compared using several plotted map components. We used the data covering the study area of CAR and visualised them for analysis of the repeated structures placed on the images and identified for the maps of gravity, geoid, topography, geology and magnetic anomalies over the CAR. The main application for such an algorithm is to perform pairwise comparison of maps where the overlap between the geological and geophysical parameters is comprised mostly of similarities in patterns on the analysed images. Our cartographic framework exploits five important characteristics of magnetic, geophysical and topographic

grids along with geological data aimed at visualising the repeated structures, depressions and extremities in the geophysical anomalies over the CAR.

We demonstrate that our cartographic framework performance in data processing works well for evaluating the coherency and feature similarity in geophysical, topographic and geological data over the CAR. Our hypothesis is that a correlation exists between the geophysical and topographic processes that are tightly connected with regional geologic structures. Such a relationship is linked to the tectonic processes that are expressed in the present land features and might be traced in the topographic surface and gravity variations. The effects of the geophysical anomalies on the distribution of the dependent variables can be observed as regional geomorphic structures. We show that our approach performs effectively for the analysis of the coherency and revealing the links between the geophysical variables in the Earth critical zone in central Africa.

1.3. Study Area

The Bangui magnetic anomaly is located in the CAR in the West Zaire Precambrian Belt (Figure 1).

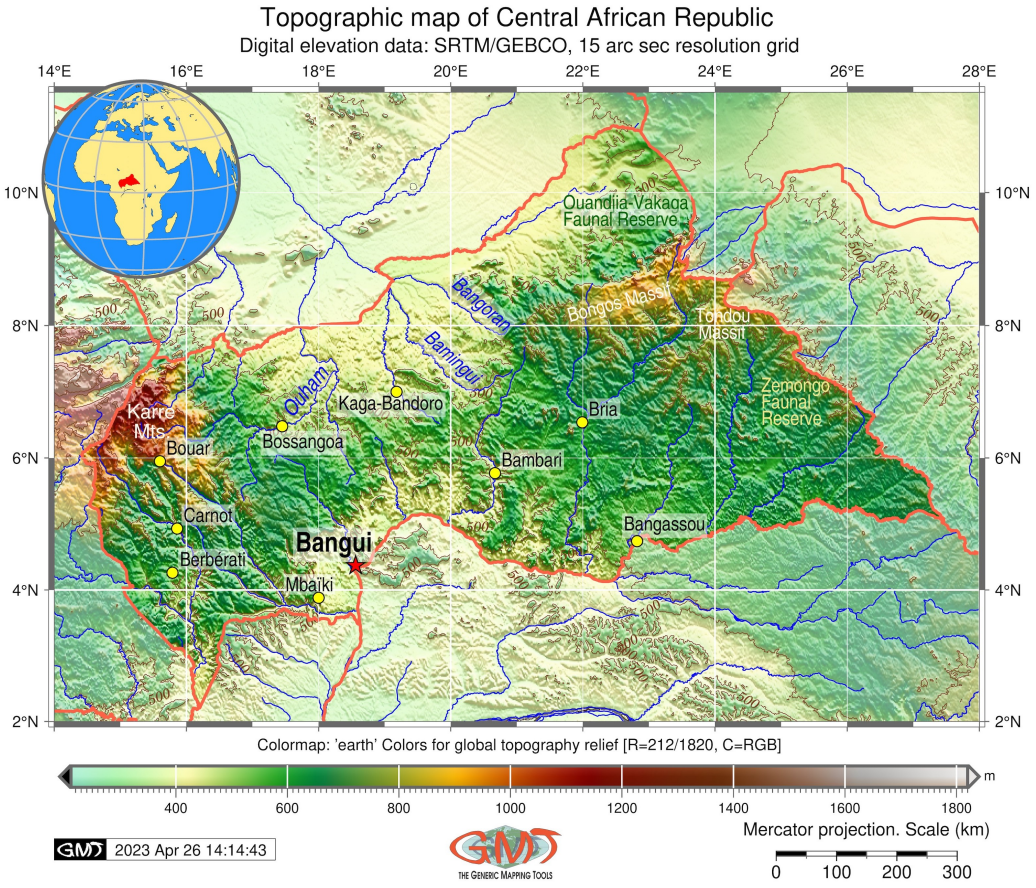

Figure 1. Topographic map of CAR.

With an amplitude of 28 nT and an area of 700,000 km^2 [21], it is the largest in Africa and one of the most important magnetic anomalies on the planet. The Bangui anomaly is named after the capital of the Central Africa Republic (CAR), located at 4°22′24″ N and 18°33′46″ E, on the right bank of the Oubangui River [22,23]. The Oubangui River is a major tributary of the Congo River and plays an important role in the economy of CAR as a key transport artery [24].

The anomaly has a crustal origin and is strongly related to the tectonic evolution and Precambrian history of the Saharan metacraton and Congo Craton, as also revealed by the satellite magnetometer data and reported in previous studies [25–27]. Geologically, it is

located in the region of the deposited highly metamorphosed Precambrian rocks and has a Precambrian basement with large masses of magmatic rocks [28]. The formation of the anomaly is related to the bending of the lithosphere. Ref. [29] reports the thick crust and a strong lithosphere beneath the anomaly, as well as high coherence between the Bouguer gravity and relief which correlates with the Moho depths near the anomaly.

At the same time, the comparison between the magnetic contrasts, geologic setting and geophysical data in the Earth's critical zones provides new insights into the formation of the continental margins and distribution of mineral resources. It furthermore allows a better interpretation of the effects of past tectonic activity on the present geophysical processes [30]. Thus, regions earlier affected by the geodynamic processes are notable for negative magnetic anomalies, which suggests a strong correlation between the active tectonics and the origin of the magnetic anomalies which is associated with the lithosphere movements [31]. For instance, ref. [32] noted that the lithosphere beneath the sedimentary basins formed during the Gondwana break up exhibits lower geomagnetism compared to the regions under the cratons, which is related to the thermal demagnetisation of the high-temperature asthenosphere. Further, certain effects are noted from the magnetic mineralogy of the ascending magma in the lower crust.

The magmatism in Central Africa is a consequence of continental rifting, opening of the Equatorial Atlantic and the Mesozoic–Cenozoic magmatic activity [33]. The lithospheric extension and the associated ascent of magma resulted in the intrusion of tholeiitic basalts which have typical geochemical and isotopic signatures. The tectonic structure of the CAR is notable for the distribution of the Central African Fold Belt which extends in the north-east direction from Cameroon through CAR towards Sudan and contributed to the tectonic magmatism. The Central African Fold Belt is formed as a result of the extension of the Congo Craton and associated collisions of the related crustal blocks in Cameroon and CAR [34]. The Mesozoic separation of African crustal blocks during the Early Cretaceous resulted in the formation of the Western Central African Rift System. As a result, crude oil deposits were formed in the structured reservoirs of the fault blocks in the rift basins of CAR [35].

The anomalies in the lithospheric magnetic field present the data on the variation in the intensity of Earth's magnetisation which indicates both explicit and hidden geophysical properties. In turn, magnetisation data reveal the properties of the underlying rock, the tectonic history of Earth and help interpret the key steps in the geologic evolution of the Earth [36]. At the same time, our understanding of these processes and the complexity of their interactions using Earth observation data can assist in practical decision making on natural resource management, sustainable environmental development and mineral exploration in the CAR.

2. Regional Geology

The geology of CAR is notable by the presence of the two prominent greenstone belts formed during the Archaean Eon as metamorphosed mafic volcanic sequences within the granite–gneiss volumes [37]. The greenstone belts are located to the north of Bouca in the West Zaire Precambrian Belt (Figure 2) as narrow subparallel bands of the extrusive igneous rocks (basalts and andesites) placed on a sialitic basement [38]. The first one is a 250-km long Bandas belt composed of volcanic and metasedimentary rocks [39] and the second is located in the west—a 150-km long Bogoin-Boali belt with anomalously high gold deposits [40]. They further include the tholeiitic basalts, dolerites from the Proterozoic dyke swarms and sills and andesites formed during crystallization of the basaltic magma [41].

The geochemistry of the greenstone belts also includes the metamorphic minerals of the greenschist facies, pyroxenes and olivines [42]. The presence of back-arc tholeiites and arc-related greywackes argues for a compressive margin plate boundary for the greenstone belts indicating high tectonic activity in the marginal areas of the Congolese Craton [43]. Further, the arc-related ultramafic origin of the bulk rocks caused by complex tectonic activity in the past, is also proved by [44] who reported on the geochemistry and petrogenesis of ultramafic

rocks in the Precambrian terrane of the northern CAR. They indicate that the presence of olivine and pyroxene, magnesio-hornblende and magnetite in the West Zaire Precambrian Belt (Figure 2) indicates intense Precambrian mafic magmatism processes in the past. The magnesian intrusive of Paleoproterozoic age is also found in the Tamkoro-Bossangoa Massif in the northwest intruded into a strike-slip shear zone. They are composed by gneisses with grained quartz diorites and biotite granites [45].

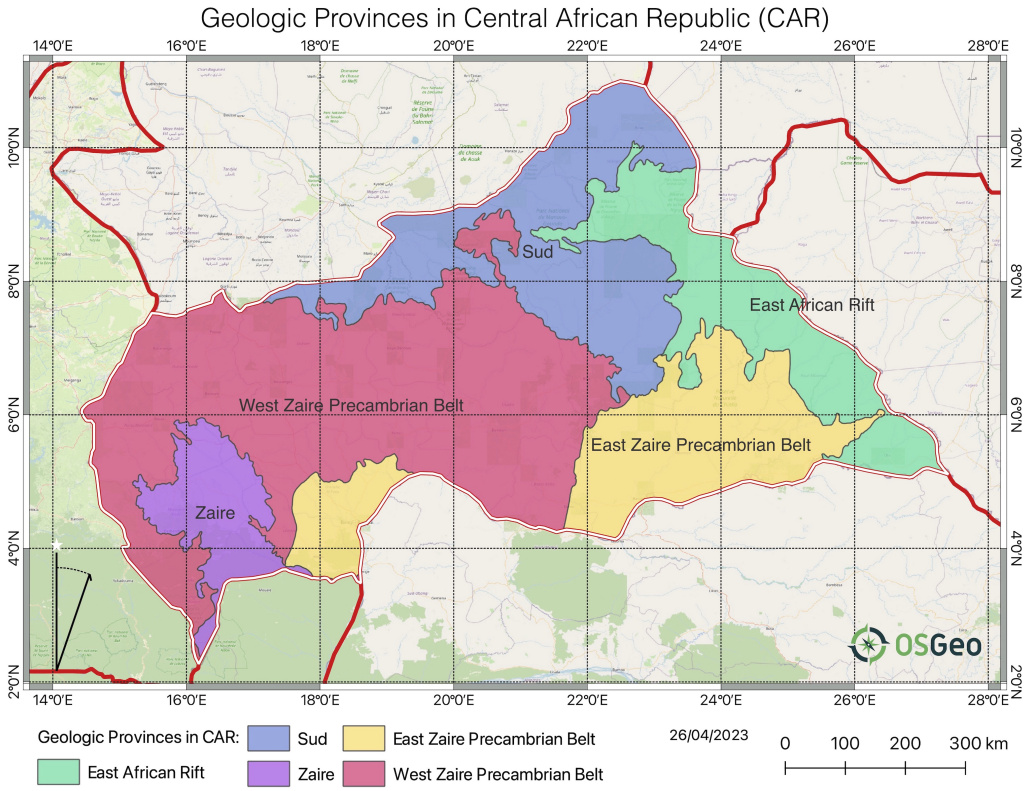

Figure 2. Geologic provinces in CAR. Data source: USGS. Background topographic map: OSGeo.

The deposits of the Bangui basin in the southern region of the CAR are dominated by the granodiorites which belong to the foreland of the Pan-African Oubanguides belt in the stratum deposited during the Proterozoic period of the Precambrian (pCm) [46]. The metamorphic rocks of the Bossangoa-Bossembélé area in the north of the country consist of the sedimentary and igneous units which are indicative of granulite facies conditions deposited on an old Paleoproterozoic continental crust [47,48]. The Precambrian carbonate platforms are widely distributed in CAR as the remaining evidence of the paleoenvironment. For instance, these include the carbonate deposits in the Ombella-M'poko Formation consisting of metamorphosed carbonate facies (calcite, dolomite and quartz) on top of the fluvioglacial sediments covered by siliciclastics [49].

Later examples of the palaeogeographic formations include the Carnot—a Mesozoic fluvio-lacustrine detrital formation located in the western part of the CAR and presented by clastic material formed before the end of the Cretaceous [50]. More details on alluvial deposits of Carnot sandstones are given in [51]. Active tectonic movements and volcanic eruptions during the Cretaceous resulted in distribution of the typical morphological bodies of the intrusives igneous rocks—dykes and sills [52].

Regional stratigraphy of the CAR is illustrated in Figure 3. The stratigraphic succession is presented by the oldest rocks from the Precambrian (Pc) and following Paleozoic (Pz) periods; the Mesozoic successions comprised of rocks from the Cretaceous (K) and Lower Cretaceous (Kl) periods; Cenozoic (QT) successions comprised of rocks from the Pleistocene (Qp), Holocene (Qe), Quaternary (Q) and Tertiary (T) periods. The Precambrian (pCm) metamorphic formation is most exposed with dominating quartzite-schistose and upper

quartzite (Bangui and Nola) series. The granitic bodies and associated gneisses of Lower Proterozoic age of Precambrian period intruding the upper series were tectonized during the period of orogeny and form the basement in the south-central CAR [53]. The greenstone belt of pCm, covered by a series of conglomerates, is distributed on a granitized gneiss basement and includes volcanites and schists [54].

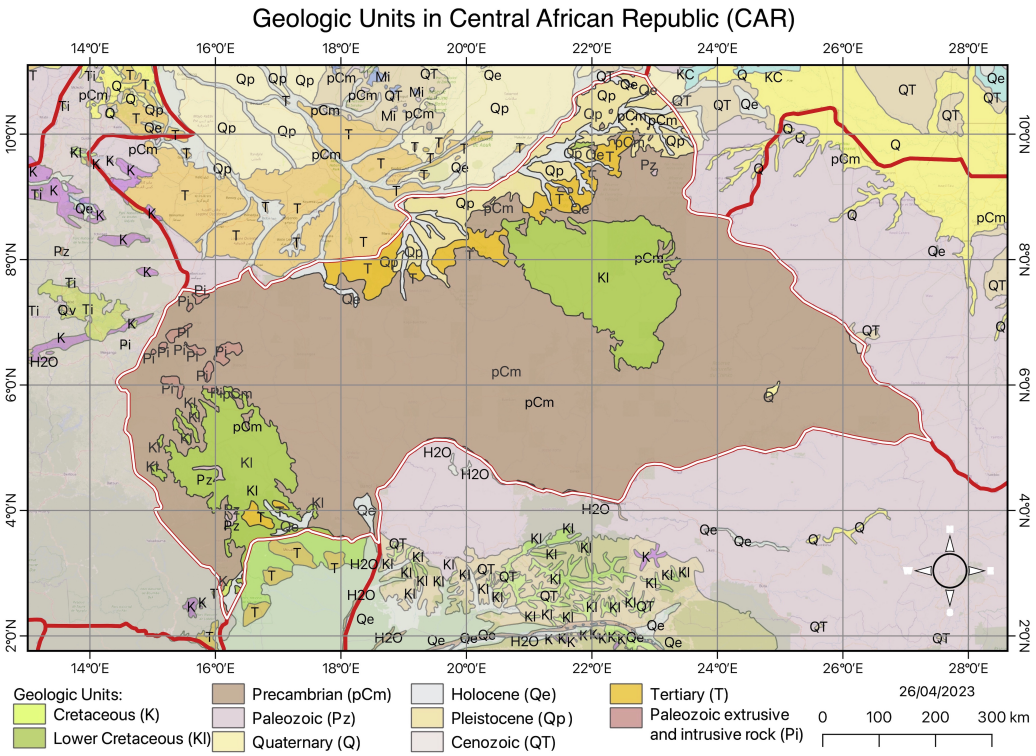

Figure 3. Geologic units and lithology in CAR. Data: USGS.

The southern region of CAR lithology continues along the northern border of the Congo Craton and is presented by the Lower Cretaceous (Kl) and Precambrian (pCm) successions (Figure 3). It is mostly composed of tholeitic basalts and gabbros of mafic and ultramafic rocks corresponding to the oceanic basalts and gabbros associated with iron-rich sediments and gneisses [55]. The Lower Cretaceous (Kl) succession, the second widely distributed in CAR, includes the fluvio-lacustrine deposits on the Central African shield [38]. Further, the interfluves of the dense fluvial network of rivers in CAR correspond to the series of plateaus with the presence of the polymorphic sandstones Tertiary (T) with the valleys composed of soft sandstone and argillites of Cretaceous (K) [56]. Further, the Bangui region is characterised by the Plutonic massifs distributed in the Ngouaka-Gbago area which include the gabbro, granodiorite, and granites that experienced the processes of the greenschist facies metamorphism [57].

The Paleozoic (Pz) period is notable for the emergence and geomorphic erosion in the earlier reliefs which resulted in the upper hilly surface of argillites in the northern regions of CAR [58]. The alluvium and colluvium from the Pleistocene (Qp) valleys with modern sediments of Holocene (Qe) form the basin of the modern Aouk river and its tributaries which create a natural border between CAR and Chad, Figure 3. The formations in the alluvial deposits also include notable intrusions of diamonds formed as a result of the ascent of the upper mantle and related magmatic processes during the geological history of CAR [59–62]. The geological development with favourable environmental setting of CAR situated in the equatorial, humid tropical and subequatorial climate resulted in its diverse natural resources. Rich mineral resources include gold-mining fields in the quartz veins in greenschist facies of the Paleoproterozoic formations [63] and alluvial diamonds [64].

The latter ones are distributed in the south-western and north-eastern regions in the Carnot and Mouka-Ouadda Sandstone formations [61,65].

The geomorphology of most of the CAR is represented by flat or hilly plateaus with dominated savannah [66] and dense ombrophile forest in the southern regions of the country [67] and the extreme northeast regions of CAR are a steppe. The northern region near the Bamingui and Bangoran rivers is presented by the Sahel-tropical forest [68]. The distribution of crops and related agriculture activities correspond to the different types of soil within various regions of the country which is in turn largely controlled by the regional setting of the geologic basement [69–71]. For instance, the organic matter in soil is controlled by the underlying geology as determining its chemical and physical nature. As a result, the extent and types of habitats and vegetation patterns vary accordingly [72,73]. Further, carbonated bed formations favour the development of karsts with typical relief and limestone soils in the southern regions of the Oubangui Basin [74].

3. Materials and Methods

This study is based on several gravity and geologic databases: two gravity databases (EMAG2 and WDMAM), satellite-derived gravity data (EGM2008) and topography data: GEBCO/SRTM [75,76], ETOPO1 [77] and IGPP [78,79]. The geologic maps were built upon the USGS data using QGIS software version 3.22.1 [80], while the other datasets were processed separately by the GMT scripts by codes presented in appendix A. The programming approaches used for mapping present an advanced alternative to the traditional cartography [81–83]. They operate with scripts which can either be used as a sequence for codes employing diverse modules used for plotting the maps [84–87], or as instruments in remote-sensing data processing [88–91].

The advantages of the presented GMT-based modular algorithms include a high level of automation in data processing. Thus, the GMT-based approach does not require generating the projects for data processing, as in traditional GIS, but instead uses the scripts and syntax of GMT. This enables researchers to perform data processing on the fly. Such an advantage enables researchers to adjust only relatively few parameters in the multi-source target datasets mapping for adaptation, textual annotations, accuracy of projections and fine-tuning in visualization. The rest is automatically performed by the script which collects the lines of GMT code and implements the workflow without much supervision, avoiding the need for human intervention as demonstrated in the scripts presented in the Appendix. Such a technical approach presents a significant benefit of GMT over the traditional GIS software and makes it a valuable instrument for geological and geophysical mapping when several datasets should be processed in an integrated way for quick and accurate cartographic data processing.

3.1. Histogram Equalisation

The equalisation of the topographic grids was determined by means of the 'grdhisteq' module of the GMT version 6.1.1 [92,93] by four different approaches in modelling elevation data: original, equalised, quadratic and normalised. The 'grdhisteq' module of the GMT models the data values and divides a grid file into the equal patches. The histogram equalisation was implemented using the topographic ETOPO1 image covering CAR with the four cases of the relief modelling. The topography was divided into the equal-area segments for approximation of the regional elevation setting using equalised, normalized, quadratic and original models. As a result, the smooth distribution of the topographic values was demonstrated using Gaussian approximation and revealed notable peaks and depressions in the elevation of CAR which are comparable with the geophysical and magnetic grids. To this end, a sequence of the different GMT auxiliary modules was used to plot the map: 'pscoast', 'makecpt', 'grdimage', 'psscale' as well as annotations added by a combination of 'echo' and 'pstext'. The parameters of the commands are defined for fine cartographic adjustments and presented as a full code as shown in Listing A1. The comparison of the processed topographic grids regularises the non-linear models in

the hypsometry of CAR to evaluate the extremities in the data covering the regions and highlights the depressions and peaks in the elevation models of the country.

3.2. Geoid

The first processing step consisted of converting the ADF file into the GDR by 'grdconvert' using the tile to the extent of CAR applied to the area of 'n00e00' in the global gravity data (Listing A2). Afterwards, the extent of the data range was evaluated for the image by the 'gdalinfo' and the visualization was adjusted by 'makecpt'. Extracting the image was done using the 'grdimage' module with the extensions applied to the actual extent of the country (−R14/28/2/11.5), that is, considering a EGM2008 clipped and extended over the target area between 14 and 28° N of parallels and 2–11.5° E of meridian. All the isolines were added on the image and interpolated with a 0.5 m step and annotations every 1 m to visualise the trends in variations of the values. To obtain the cartographic grid, ticks and annotations of graticule, the 'psbasemap' module was used with relevant parameters adjusted by flags, as shown in Listing A2. The GMT script written for plotting the geoid and demonstrated in Listing A2 was used as the basis for plotting the maps of topography, and vertical gravity gradient in CAR with adjusted elements in codes and changed datasets processed in scripts, accordingly.

3.3. IGPP Earth Free-Air Anomaly

Gravity data were extracted from the EGM2008 database with global coverage resulting from the spherical harmonic models of the Earth's gravitational potential by [79]. Diverse data-processing algorithms were applied using the GMT modules as shown below in Listing A3. The raster image was visualised using the 'grdimage' modules with isolines added as contours with 20 m interval by the 'grdcontour' module. The visualization was adjusted for gravity grid to better represent the variations in the geophysical data. The colour palette was adjusted according to the amplitude and geometry of the observed values in the raster grids, which were checked using the 'gdalinfo' module. The remaining cartographic elements were added using the sequence of modules GMT such as 'psbasemap', 'pscoast', 'pstext' and more, as demonstrated in Listing A3.

3.4. Coherency of Geophysical Grids

The 'grdfft' module that couples different grids and performs the computation on the grids in a frequency domain using Fast Fourier Transform (FFT), the coherency between the vertical gradient and free-air gravity anomaly was plotted and visualised along with the grids on magnetic, topographic and gravity data. The comparison of several maps allows the analysis of the correspondence of the crustal structure in the CAR region, the estimation of the topographic heights and hypsometry, and the coherency between the gravity and vertical gravity gradient. Such data integration allows better understanding of the geophysical and topographic responses on the inner behaviour of the lithosphere and geologic structure of CAR region, and their correspondence with the magnetic contrasts. The analysis of the coherency used for plotting the graph was performed using the GMT module 'grdfft' which processes the data using FFT, estimates the cross-spectral for the co-registered gravity grids (mGal), and reports the result as functions of the symmetry reflection between the both grids. To this end, the data were compiled and processed using the code in Listing A4.

4. Results

In this section, we present the results of this study which we briefly summarize as follows: (1) maps of the geologic structure and units in the region of CAR enabled us to analyse the correlation between the geological and geophysical setting; (2) maps of the gravity and geoid variations for estimation of the contrasts; (3) coherence between the vertical gravity anomalies and gradient; (4) visualisation of the extent of the magnetic anomalies for analysis of the correspondence with the lithosphere structure of CAR based on

the datasets on geologic provinces and units; (5) histogram equalisation of the topography grids on CAR based on the ETOPO1 raster data for analysis of topographic setting, Figure 4.

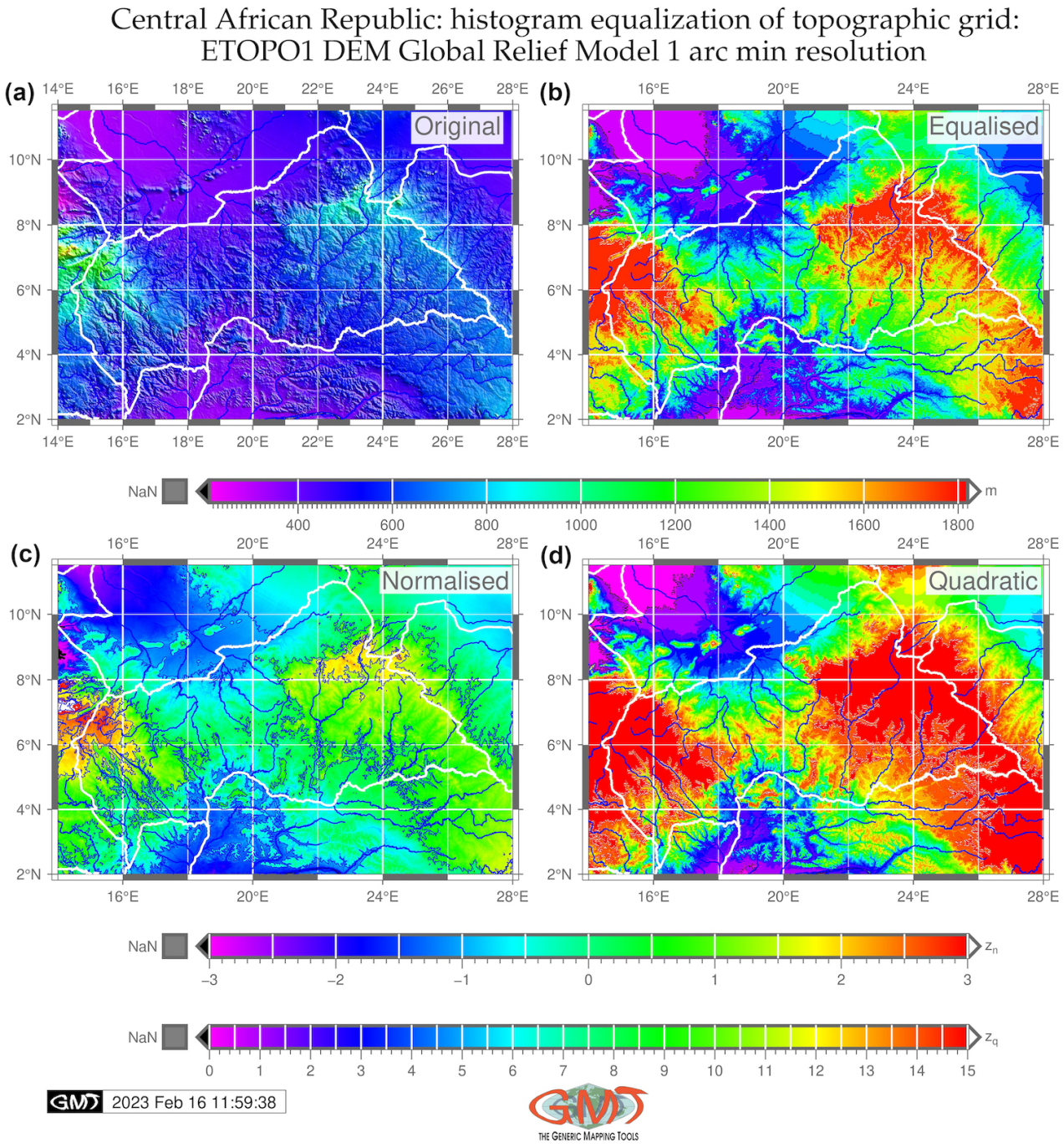

Figure 4. Histogram equalisation of the topography grids on CAR based on the ETOPO1 raster data. (**a**) original grid; (**b**) equalised grid; (**c**) normalised grid; (**d**) quadratic grid. Data source: ETOPO1.

The analysis of the topographic grid reveals a local depression in the equalised raster grid which corresponds to the geoid and gravity data in the central region of CAR. Furthermore, the data are contrasted in the equalised and quadratic models (Figure 4b,d) compared to the original and normalised grids (Figure 4a,c), where topographic derivatives reveal a saddle-shaped structure in the 1 min topographic ETOPO raster in the region of the magnetic anomaly. This proves the distribution of the ring-shaped formation around the region of magnetic anomaly that has an outer-ring diameter of over 810 km and an inner-ring diameter of 490 km, which is confirmed by [21].

The gravity anomalies are caused by the rugged surface, and non-linear and complex composition of the Earth's inner structure. Other factors include thinner lithospheric thickness and Moho depths associated with the isostatic surface topography [94] which affects its gravitational field. Furthermore, the values of gravity are affected by the rotation of the Earth which results in values near the equator being higher compared to those on the poles. Beneath the magnetic anomaly, the geoid in CAR has values ranging from −4 to −8 m, which is lower compared to that of the western region where values above 16 m were recorded. Moreover, the change in the geoid undulations over the elevations compared to the topographic depressions might be affected related to the plate tectonics and the processes of cooling lithosphere, thermal conductivity and mantle mineralogy [95].

The geoid height is sensitive to the distribution of density in the Earth's mantle which explains the variations with higher values in the south-western region of CAR and negative values in the eastern regions (Figure 5). Furthermore, the contrasts in values of the geoid are influenced by the lithospheric heterogeneities [96] which pose constraints in the density material that are reflected in the surface variations of geoid [97].

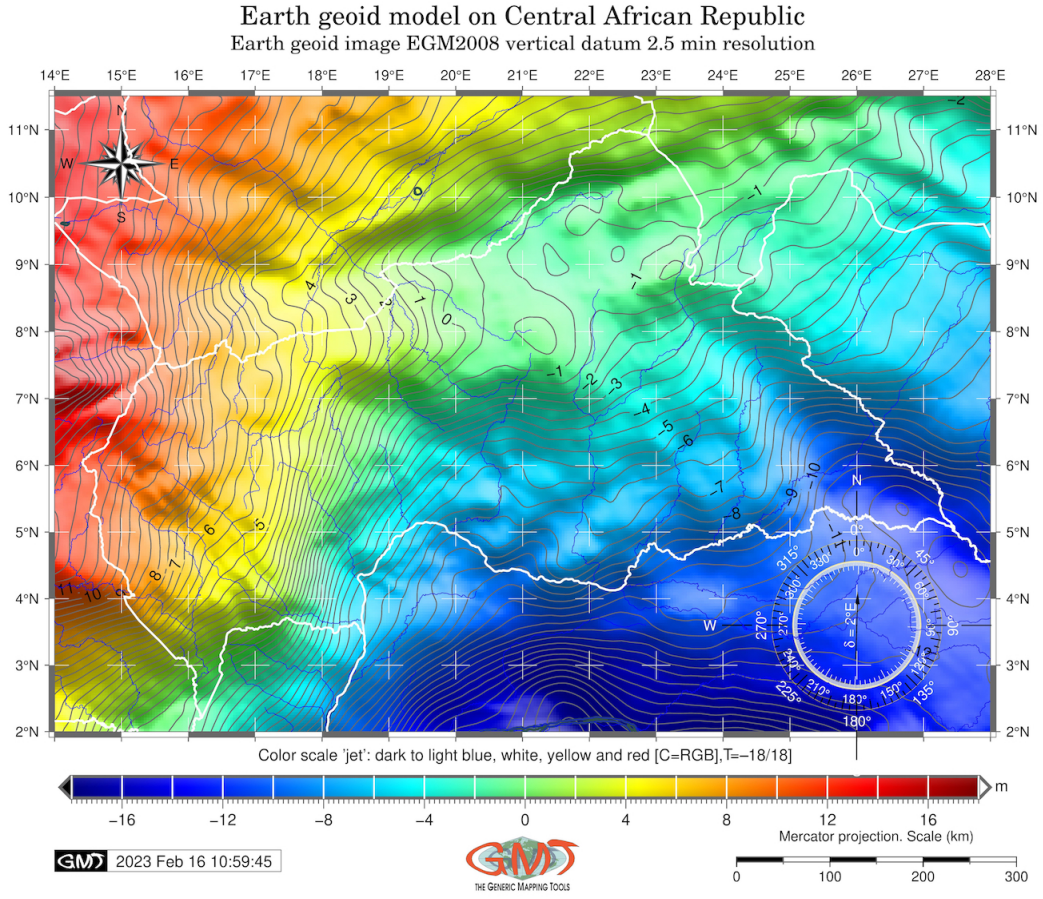

Figure 5. Earth geoid map of Central African Republic. Data source: EGM2008 Global Earth Geoid [79]. Magnetic declination (magnetic rose in lower right corner) is given for Votofo, CAR: +1.63° (east, positive).

The geoid grid was mapped and compared with the magnetic anomaly in the Bangui area (Figure 5) to show the coherency with structural variations in the crust reflected in the gravity values of geoid. Thus, the distribution of the magnetic contrasts continues up to a depth of 160 km where the crustal thickness is about 40 km [98], indicating a close relation between the Bangui magnetic anomaly and of the geoid and geophysical data that result in similar contrast patterns due to the Panafrican orogenic events [99]. Since the Bangui magnetic anomaly continues within the Central African Orogenic Belt, which is a subject of the cumulative effects of the multiple tectonic events during the geological development in

Precambrian and later periods, it has a thin lithosphere structure beneath the anomaly that well correlates with the gravity data [100].

Gravity anomalies and amplitude contrasts (Figure 6) result from the lower lithospheric depth and crustal density which correspond to the heterogeneities in the mantle density [101]. As a result, similar gravity patterns at the surface closely follow the tectonic structure in the Central African Orogenic Belt due to the active mantle flow and thermal convection [102]. The analysis of Figure 6 corresponds to the earlier maps [103] and reveals negative values from −80 to −60 mGal over the study area (Figure 6). In contrast, higher values over +50 mGal are clearly visible in the western and southwestern regions of CAR that correspond to the regional outcrops of the Lower Cretaceous rocks (Figure 3) in the Zaire geologic province (Figure 2).

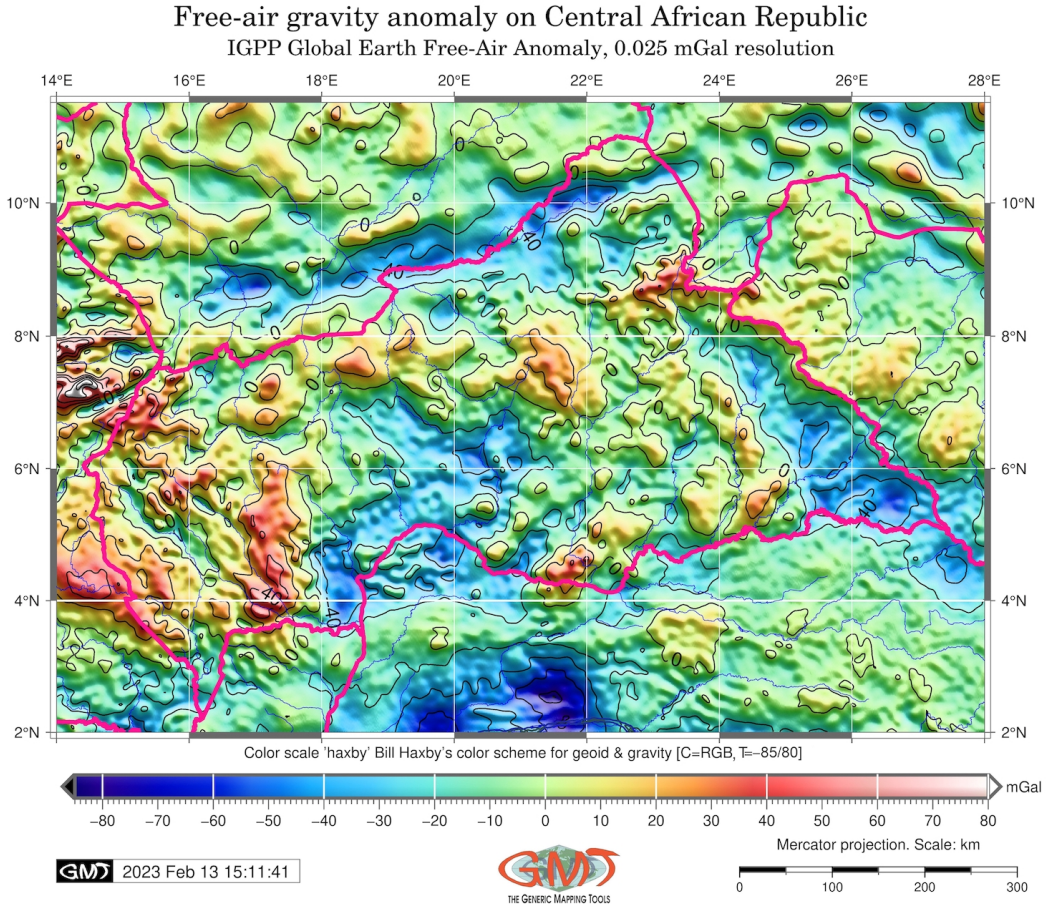

Figure 6. IGPP Earth Free-Air Anomaly on Central African Republic. Data source: EGM2008.

The geologic structure in this region includes the Paleozoic glacial clastic sedimentary formations which are formed, among others, by tillites, argillites and mudstones cropping out from several sedimentary formations [104]. The comparative analysis of Figures 6 and 7 with data on magnetic anomaly shows that negative Bouguer anomaly of ca. −40 mGals (blue colours in Figure 6 and dark blue areas in Figure 7) coincides with the distribution of the magnetic anomaly, which implies that these heterogeneities are related to the Earth lithosphere and geologic features increasing or depreciating local magnetic field depending on the subsurface structure and composition of the Earth's crust. Furthermore, the variations in vertical gravity intensity observed in Figure 7 highlight the difference in lithospheric mass anomalies caused by deeper density contrasts.

Surface topography is strongly related to geologic–tectonic processes, and at the scale of this study, is more affected by erosion than other causes. Additionally, it is also associated with seismic anomalies in the dense mantle [105]. In turn, seismic velocity anomalies are proportional to the heterogeneities in mantle density related to the tectonic activities [106].

Therefore, the observed geoid heights over cratons differ in gravity values than in the region of the magnetic anomaly and the distribution of the related Central African Orogenic Belt. For instance, major structural elements in the Bossangoa and Bossembele areas in the northwest reflect the tectonic evolution of the basement of the North Equatorial fold belt, which includes the shear zones, lineations and fold axes [107] that affect the shape of the geoid and topography in the modern relief of CAR. As a result, gravity values affected by the crustal density and continental lithospheric thickness are reflected in the topography and the geoid patterns of CAR.

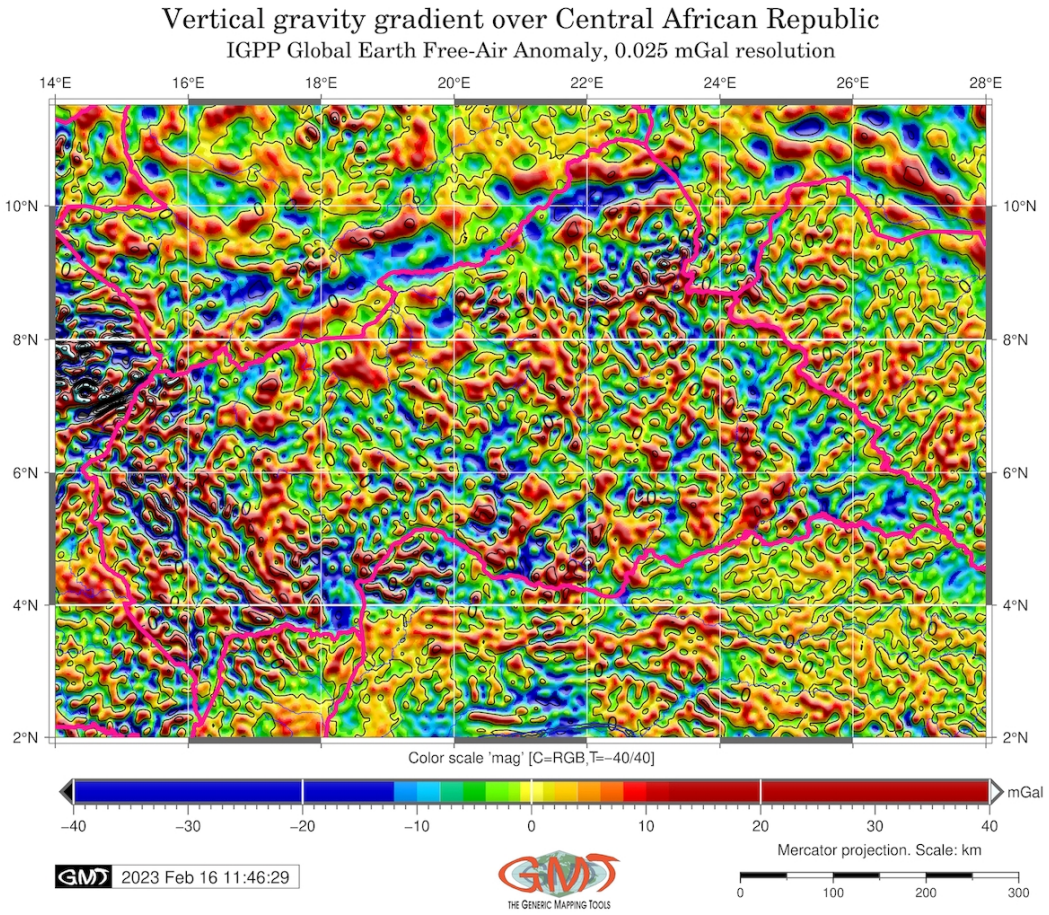

Figure 7. Derivative of the IGPP Earth's gravity field on Central African Republic: vertical gravity gradient. Data source: EGM2008 Global Earth Geoid [78].

The distribution of the bipolar magnetic anomaly has the major part of its negative values over two-thirds of the CAR in the central and south-west regions of the country. It also shows a distinct large negative depression with values greater than 1000 nT and surrounding peaks which well correspond with previous records [108]. The negative values are visualised as dark blue colours (Figure 8) while the peaks are visible in the northern regions of the country with corresponding values of 300 to 400 nT (dark red colours in Figure 8). Moreover, these data conform to records from the Magsat, a satellite specifically used for the measurement of the crustal magnetic anomalies of the Earth. It shows the existing correspondence between the magnetic data and the surface geology and tectonics in central Africa [109]. The magnetic intensity (Figure 8) compared with the Central African geologic and gravity maps (Figures 2–4) shows that most of the geologic units and geophysical patterns are reflected by the magnetic fields which proves the interrelation between the topography and the geologic structure with the magnetic field data over CAR.

Lower magnetic values are observed across the gneissic and granitic rocks of the shields and across the greenstone belts of CAR. Furthermore, they correspond to the area over the greenstone belt intruded by the Precambrian rocks with ultrabasic dykes. In con-

trast, the extent of the East Africa Rift correlates with the moderate magnetic values which lie between −20 and 10 nT (corresponding to yellow colours in the map of Figure 8) and from +20 to +40 nT in the north-east region of the country (soft orange colours in Figure 8) in Sud geologic Province with Pleistocene outcrops. The highest magnetic values over +60 nT (bright red colours in Figure 8) correspond to the distribution of the Precambrian rocks in the south and occasional Tertiary rocks in the north of the country. The most heterogeneous pattern of the magnetic data is visible in the West Zaire Precambrian Belt, where the lowest depressions of the dataset contrast with the highest peaks in values (Figure 8 cf. Figure 2).

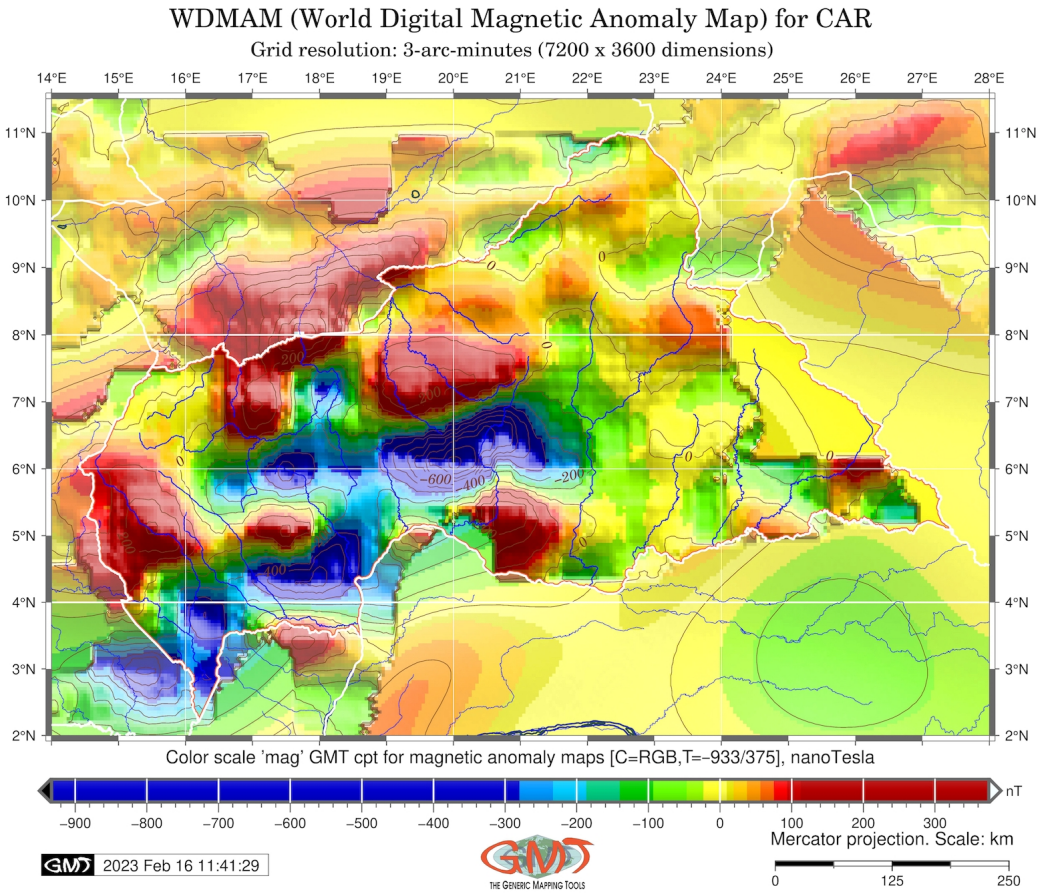

Figure 8. Magnetic anomaly in CAR based on WDMAM with 3-arc-minute resolution. Dark blue areas indicate the negative Bangui magnetic anomaly in the centre of CAR. Data source: WDMAM [110].

Figure 9 shows a detailed view of the anomaly derived from the 2-arc-minute resolution grid. It reveals that the Bangui anomaly consists of three separate segments with a large central negative anomaly having elongated shape and two with positive anomalies situated to north- and southwards of the large negative depression. The Bangui magnetic anomaly derived from the EMAG2 grid illustrates a typical interpolated pattern of the magnetic anomalous field, magnetised by induction in a zero inclination field [111]. As the magnetic equator passes near the centre of the surface, the computed-based modelling reveals the distribution of the negative and positive values in the Bangui anomaly accordingly. Certain trends exist in the data on the daily amplitude of the magnetic variation in the Bangui magnetic anomaly which demonstrated fluctuations over the long-term period [112,113]. These revealed possible fluctuations in the Earth's magnetic field that might be affected by the ionospheric conductivities. However, the visualised dataset is based on the EMAG2 grid which is compiled from the remote-sensing observations obtained from satellite, ship, and airborne magnetic measurements with improved resolution to 2-arc minutes [114].

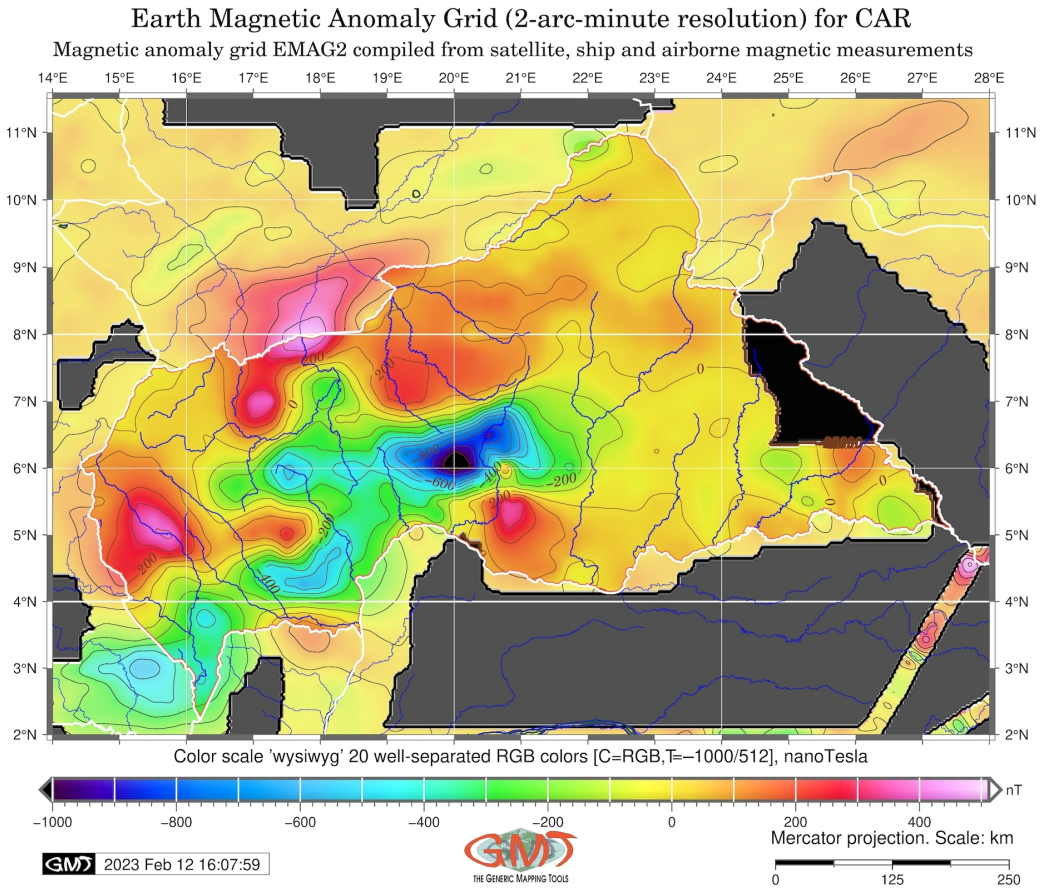

Figure 9. Magnetic anomaly in CAR based on EMAG2 with 2-arc-minute resolution. Dark blue area indicates the negative Bangui magnetic anomaly. Black and dark grey areas represent the "no data" areas where no magnetic survey was performed in the original dataset. Data source: EMAG2 [115].

Figure 10 demonstrates the coherency between the geophysical data, hypsometry and the Bangui magnetic anomaly fields. Thus, the gravity data with −120 mGal Bouguer anomaly, the associated negative depressions in the geoid derived from the EGM2008 and the ETOPO1-based topographic hypsometry over CAR all correlate with the negative values of the Bangui magnetic anomaly that are below −1000 nT. At the same time, the comparison of the extent of the Bangui magnetic anomaly (Figures 8 and 9 with an enlarged view in the composed plot shows the coherency with geophysical data, and the geologic maps of CAR (Figures 3 and 4) demonstrates the predominant distribution of the Precambrian (pCm) rocks in this critical region that are exposed just under the central area of the magnetic anomaly and depressions in gravity. The spatial extent in the grids (Figure 10) showing combined magnetic and Bouguer gravity data (WDMAM, EGM2008, IGPP and EMAG2) indicates the integrity of the geophysical and geomagnetism in CAR.

The correlation is visible between the lowest magnetic data in the region from 3° N to 7° N (white rectangle in Figure 10) and the elongated negative depression in the free-air gravity at 4° N over the basement of West Zaire Precambrian Belt which has a south-west-north-east extension over the territory of CAR. Such correspondence is related to the variations in crustal thicknesses in this region of CAR caused by the tectonic processes.

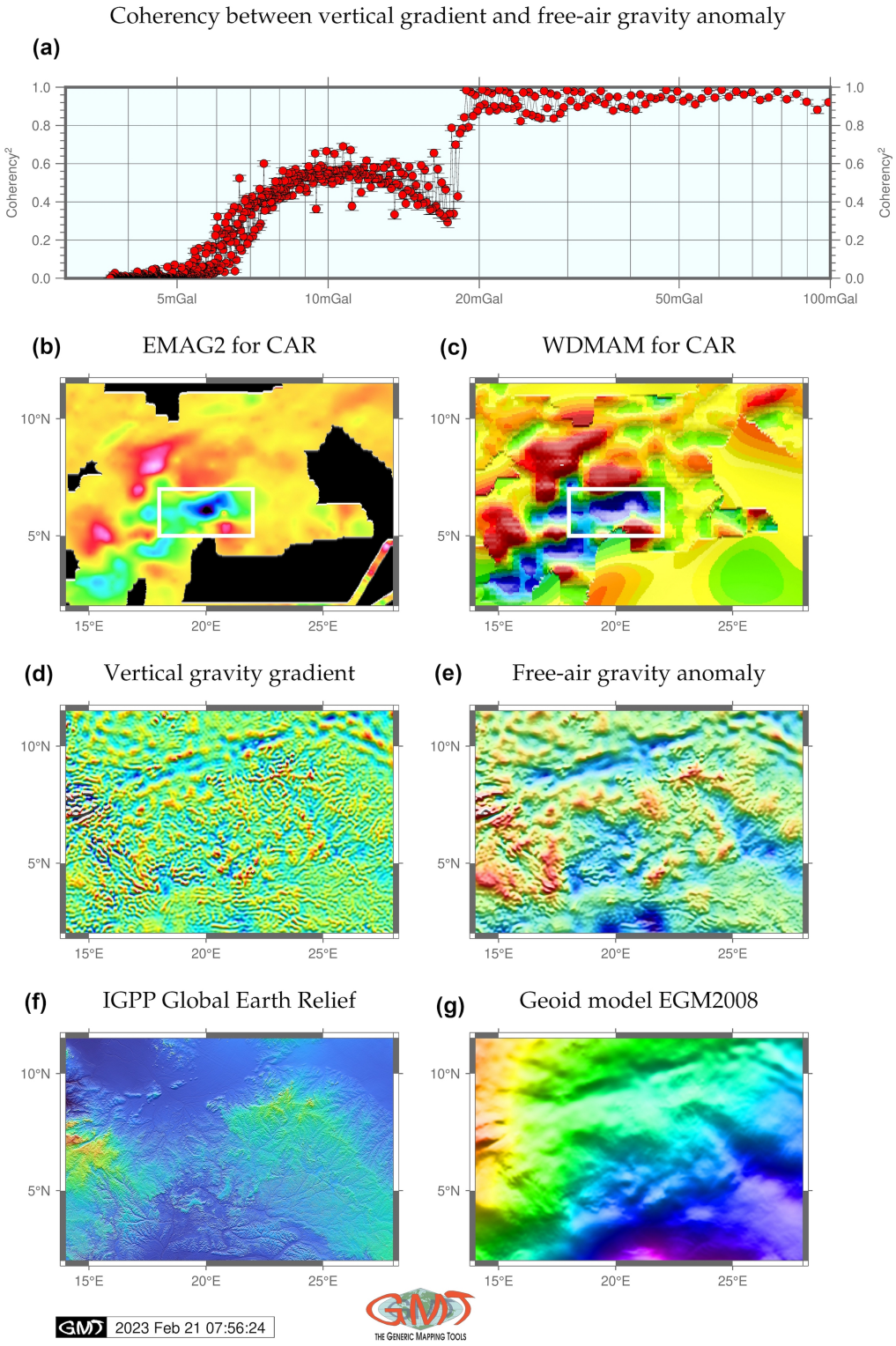

Figure 10. Coherency between the geophysical grids on CAR. (**a**) Coherency between the vertical gravity and free-air gravity anomaly grids on CAR; (**b**) Magnetic anomalies on CAR based on the EMAG2 grid; (**c**) Magnetic anomalies representing the WDMAM grid; (**d**) Vertical gravity gradient; (**e**) Free-air gravity anomalies over CAR; (**f**) Relief model based on the IGPP; (**g**) Geoid model based on the EGM2008.

This highlights the interrelation of gravity anomalies with amplitudes ranging from −85 to +80 mGal over CAR with negative values beneath the magnetic anomaly. Such

contrasts indicate the extent of the major tectonic structures of CAR: the Central African Orogenic Belt on the Precambrian shield and the northern part of the Congo Craton.

5. Discussion

Detecting patterns in the lithospheric structure using the integrated mapping of gravity, magnetic fields, geoid and topography data is of paramount interest for the Earth sciences. Accordingly, we examined the relationship between these datasets over CAR via the advanced cartographic approach. To this end, we presented a GMT-console-based method of the cartographic data processing, which was integrated into the geological–geophysical analysis of the Bangui magnetic anomaly and surrounding regions. We tested our proposed techniques in the context of the regional setting of CAR, where an extreme magnetic anomaly is present in the Bangui area. Overall, seven datasets are processed, visualised, evaluated and analysed including the geoid EGM2008, IGPP, GEBCO, ETOPO1, EMAG2, WDMAM and the geologic datasets obtained from the USGS.

The coherency between the geologic structure of CAR and geophysical datasets was determined by means of the multi-source datasets using diverse modules of GMT to assess the regions crossed by the Bangui magnetic anomaly. Based on the conceptual GMT-based cartographic framework developed for the study, we confirm the hypothesis derived from the obtained new maps on CAR. Considering the local geological and geophysical context of CAR, we answer the defined research questions as follows: (Q1): The Bangui magnetic anomaly is positively associated with gravity values and free-air anomaly. (Q2): The Bangui magnetic anomaly is associated with the distribution of the geologic setting in the region of CAR.

The results show that the gravity structures and the hypsometry associated with the Bangui magnetic anomaly are strongly linked with the extent of the major geologic units and tectonic structures including Central African Orogenic Belt and the northern part of the Congo Craton. As a continuation of this work in the future, three directions are possible. First, the integration of other datasets including remote-sensing data. Second, an extension of the current methods of cartographic scripting by other modules of GMT. Third, extension of the study area towards the neighbouring regions of Africa for further geological analysis. Furthermore, the estimated values of the magnetic lowest negative values between -1000 nT and -280 nT were compared to the extent of the topographic and geophysical grids to reveal correlations between the datasets. The obtained results are demonstrated on the presented maps, showing that gravity contrasts are related to the extent of the magnetic anomaly which are tightly connected to the tectonic structures and geologic data on CAR.

This study presented a previously unpublished analysis of the coherence between the geophysical and geomagnetic data over CAR implemented via the GMT scripts. Limited information on the Bangui magnetic anomaly and scarce data on its relationship with regional geologic setting, lithospheric structure and gravity motivated this research and underlined the actuality of the presented results. In this regard, mapping the magnetic and gravity anomalies over CAR, analysed in the context of its regional geologic and tectonic development contributes both to the theoretical investigation on geotectonic and geological setting in central Africa and to the practical increase of geospatial information aimed at mineral exploration in CAR. With respect to the practical geologic aims and management of natural resources, mapping the coherency between the Bangui magnetic anomaly, geophysical data and geologic setting contributes to the analysis of the Earth's structure and further knowledge over the geophysical and geological settings in central Africa.

6. Conclusions

The study contributes to the literature in the following aspects. First, the understanding of associations is broadened between the Bangui magnetic anomaly and geophysical and topographic settings of CAR based on a cartographic analysis. Second, the effects of gravity and geological setting on the distribution of the anomaly are considered. Third,

the coherency between gravity grids modelled the extent to which the data are associated with vertical gradient and free-air gravity anomaly. Fourth, the topographic grids were investigated by histogram equalisation of datasets over CAR to highlight the effects among altimetry in the study region. Consequently, the study revealed and highlighted the extent to which the Bangui magnetic anomaly, geophysical setting, altimetry as height altitude, geoid model, and distribution of the geological are associated. The correlations and coherence between these data were organised in a cartographic and structural analysis framework.

Thus, this study describes the correlation between the distribution of rocks with high magnetism in the central part of the Bangui anomaly of CAR, geologic fields of granites, greenstone belts, and the metamorphosed basalts as rock exposures. Moreover, the data were presented and compared regarding the extent of the negative Bouguer anomaly below the -80 mGal with low geoid values, as well as the distribution of the magnetic contrast with abnormally negative values ranging in amplitude between -1000 and -200 nT. The scripts used by the GMT modules were adapted to each processed image for a semi-automatic technical workflow, allowing for the comparison of these data. The experimental applications of the GMT scripts validated the suitability and effectiveness of the proposed method in different tasks of the multi-source geospatial data processing.

From a cartographic perspective, we proposed an advanced framework for mapping several geospatial datasets using the GMT scripts to reveal the coherency between geophysical and topographic data. We evaluated the distribution of values in topographic, gravity and magnetic contrasts over CAR using several multi-source high-resolution datasets: EMAG2, WDMAM for magnetic anomalies, GEBCO/SRTM and ETOPO1 for topography, IGPP for gravity grids, EGM2008 for geoid undulations and the USGS data on the geology of CAR. Our experiments show that the scripting approach of GMT reduces the workload of mapping compared to the GIS while obtaining print-quality maps. Our approach is flexible enough to deal with multi-source datasets of various formats and origin as well as rapid plotting of several maps in the identical projection and spatial extent for comparability. The detailed analysis of maps supports a more detailed investigation of the effects of geophysical and geological setting on the distribution of the Bangui magnetic anomaly.

To the best of our knowledge, there is no similar study in the existing literature that integrates the data on geophysical and geologic settings on CAR. As discussed in previous sections, the existing scarce studies on the geophysical setting of CAR mostly employed the GIS for mapping the geology and magnetic data. Therefore, the current study presented previously unpublished data, maps and results of spatial analysis based on the integrated geophysical data over the magnetic anomaly in the Bangui area, CAR. To understand the effects of gravity anomalies and geological fields on the distribution of the magnetic magnetic anomaly in the Bangui area, we present a series of previously unpublished maps supported by spatial analysis. The association between the decrease in magnetic values based on the EMAG2 and WDMAM with gravity, geologic and topographic data are revealed and discussed.

The present study contributes to the Earth studies in central Africa by providing geologists with novel series of maps increasing knowledge of geophysical and geological data in the CAR, where scarce studies are noted. As such, this paper adds to current knowledge of the CAR region by presenting an integrated approach of mapping the multi-source geophysical, topographic and geological data with repeated structures. In particular, we analysed the coherency of the Bangui magnetic anomaly with gravity and topography data. Similar features in geological and geophysical data were identified and the correlation of the data distribution was discussed to add information in the existing geophysical studies on CAR. The study objectives were implemented and tested on open data from publicly available geophysical and topographic grids. Analysing the results, we note a comparability in the distribution of geophysical and magnetic data over CAR, caused by links between the processes related to the inner geophysical processes in the Earth's crust and the topographic structure. Specifically, the paper demonstrated that the geologic

setting, and geophysical and topographic structures affected the distribution of the Bangui magnetic anomaly, and the data are associated with regional altimetry.

In conclusion, this study investigated factors associated with the extent, intensity and distribution of the Bangui magnetic anomaly based on a data analysis obtained from a novel series of maps. On the presented new maps, we have shown that the distribution of the Bangui magnetic anomaly correlates with the negative values in gravity and geoid as well as local depressions in a regional topography of CAR. The analysis of the correlation between the data revealed a non-linear relationship between past tectonic evolution and present geophysical processes, reflected in local variations of regional topography and gravity around the magnetic anomaly. In addition to the analysis of coherence of the geological and geophysical datasets on CAR, this paper discussed the aspects of the GMT-based mapping with scripts provided as a technical reference. Spatial analysis in Earth sciences relies on data representation in the form of maps. Therefore, advanced mapping techniques support geological studies by providing new information that reveals hidden structures on the Earth's surface.

Author Contributions: Supervision, conceptualization, methodology, software, resources, funding acquisition, and project administration, O.D.; writing—original draft preparation, methodology, software, data curation, visualization, formal analysis, validation, writing—review and editing, and investigation, P.L. All authors have read and agreed to the published version of the manuscript.

Funding: The publication was funded by the Editorial Office of Minerals, Multidisciplinary Digital Publishing Institute (MDPI), by providing 100% discount for the APC of this manuscript. This project was supported by the Federal Public Planning Service Science Policy or Belgian Science Policy Office, Federal Science Policy—BELSPO (B2/202/P2/SEISMOSTORM).

Institutional Review Board Statement: Not applicable.

Informed Consent Statement: Not applicable.

Data Availability Statement: Not applicable.

Acknowledgments: The authors thank the three anonymous reviewers for reading and providing useful comments which improved the initial version of this manuscript. The GMT [92] and QGIS [80] software packages were used extensively in the preparation of this paper.

Conflicts of Interest: The authors declare no conflict of interest.

Abbreviations

The following abbreviations are used in this manuscript:

CAR	Central African Republic
CGMW	Commission for the Geological Map of the World
EGM2008	Earth Gravitational Model 2008
EMAG2	Earth Magnetic Anomaly Grid
ETOPO1	Earth Topography Model with 1-arc-minute resolution
FFT	Fast Fourier Transform
GEBCO	General Bathymetric Chart of the Oceans
GMT	Generic Mapping Tools
IAGA	International Association of Geomagnetism and Aeronomy
IGPP	Institute of Geophysics and Planetary Physics
SRTM	Shuttle Radar Topography Mission
USGS	United States Geological Survey
WDMAM	World Digital Magnetic Anomaly Map

Appendix A. GMT Scripts

Appendix A.1

Listing A1. GMT script for computing the histogram equalisation of CAR's topographic grids.

```
#!/bin/bash
gmt grdcut ETOPO1_Ice_g_gmt4.grd -R14/28/2/11.5 -Gcf1_relief.nc
ps=HistCAR.ps
gmt makecpt -Crainbow -V -T212/1820 > t.cpt
gmt makecpt -Crainbow -T0/15/1 > c.cpt
# 1 upper left plot
gmt grdhisteq cf1_relief.nc -Gout.nc -C16
gmt grdimage cf1_relief.nc -I+a45+nt1 -Ct.cpt -JM3i -Y6i -K -P \
    -Bpxg4f1a2 -Bpyg4f2a2 -Bsxg2 -Bsyg2 -BWSNe > $ps
echo "24 10 Original" | gmt pstext -Rcf1_relief.nc -J -O -K -F+jBL+f12p -T
    -Gwhite@10 -Dj0.1i >> $ps
gmt pscoast -R -J -Ia/thinner,blue -Na -N1/thick,white -W0.1p -Df -O -K >>
    $ps
# 2 upper right plot
gmt grdimage out.nc -Cc.cpt -J -X3.5i -K -O \
    -Bpxg4f2a4 -Bpyg4f2a2 -Bsxg2 -Bsyg2 -BWSNe >> $ps
gmt pscoast -R -J -Ia/thinner,blue -Na -N1/thick,white -W0.1p -Df -O -K >>
    $ps
echo "24 10 Equalized" | gmt pstext -R -J -O -K -F+jBL+f12p -T -Gwhite@10 -
    Dj0.1i >> $ps
gmt psscale -Dx0i/-0.4i+jTC+w5i/0.15i+h+e+n -O -K -Ct.cpt -Bg200f10a200 -By
    +lm >> $ps
# 3 low left plot
gmt grdhisteq cf1_relief.nc -Gout.nc -N
gmt makecpt -Crainbow -T-3/3 > c.cpt
gmt grdimage out.nc -Cc.cpt -J -X-3.5i -Y-3.0i -K -O \
    -Bpxg4f2a4 -Bpyg4f2a2 -Bsxg2 -Bsyg2 -BWSNe >> $ps
gmt grdcontour cf1_relief.nc -R -J -C200 -A500+f7p,26,blue -Wthinnest,blue
    -O -K >> $ps
echo "23.5 10 Normalized" | gmt pstext -R -J -O -K -F+jBL+f12p -T \
    -UBL/-5p/-4.0c -Gwhite@10 -Dj0.1i >> $ps
gmt pscoast -R -J -Ia/thinner,blue -Na -N1/thick,white -W0.1p -Df -O -K >>
    $ps
# 4 low right plot
gmt grdhisteq cf1_relief.nc -Gout.nc -Q
gmt makecpt -Crainbow -T0/15 > q.cpt
gmt grdimage out.nc -Cq.cpt -J -X3.5i -K -O \
    -Bpxg4f2a4 -Bpyg4f2a2 -Bsxg2 -Bsyg2 -BWSNe >> $ps
gmt pscoast -R -J -Ia/thinner,blue -Na -N1/thick,white -W0.1p -Df -O -K >>
    $ps
echo "24 10 Quadratic" | gmt pstext -R -J -O -K -F+jBL+f12p -T -Gwhite@10 -
    Dj0.1i >> $ps
gmt psscale -Dx0i/-0.4i+w5i/0.15i+h+jTC+e+n -O -K -Cc.cpt -Bg0.5f0.1a1 -By+
    l"z@-n@-" >> $ps
gmt psscale -Dx0i/-1.0i+w5i/0.15i+h+jTC+e+n -O -K -Cq.cpt -Bg0.5f0.2a1 -By+
    l"z@-q@-" >> $ps
gmt logo -Dx0.0/-4.5c+o-1.0c/0.2c+w2c -O -K >> $ps
gmt pstext -R0/10/0/15 -JX10/10 -X-8.0 -Y6.5c -N -O \
-F+f14p,Palatino-Roman,black+jLB >> $ps << EOF
0.0 11.5 Central African Republic: histogram equalization of topographic
    grid:
1.5 10.7 ETOPO1 DEM Global Relief Model 1 arc min resolution
EOF
gmt psconvert HistCAR.ps -A0.5c -E720 -Tj -Z
```

Appendix A.2

Listing A2. GMT script for mapping the Earth geoid model on CAR.

```
#!/bin/bash
gmt grdconvert n00e00/w001001.adf geoid_CF.grd
gdalinfo geoid_CF.grd -stats
```

```
gmt makecpt -Cjet.cpt -T-18/18 > colors.cpt
ps=Geoid_CF.ps
gmt grdimage geoid_CF.grd -Ccolors.cpt -R14/28/2/11.5 -JM6.5i -P -Xc -I+a15
    +ne0.75 -K > $ps
gmt grdcontour geoid_CF.grd -R -J -C0.5 -A1.0+f8p,0,black -Wthinner,dimgray
     -O -K >> $ps
gmt psbasemap -R -J --MAP_FRAME_AXES=WEsN \
    --FORMAT_GEO_MAP=ddd:mm:ssF \
    --MAP_GRID_CROSS_SIZE_PRIMARY=0.8c \
    --MAP_GRID_CROSS_SIZE_SECONDARY=0.5c \
    -Bpx1f1a1 -Bpyg1f1a1 -Bsxg1 -Bsyg1 \
    -B+t"Earth geoid model on Central African Republic" -O -K >> $ps
gmt psscale -Dg14/1.5+w16.0c/0.15i+h+o0.3/0i+ml+e -R -J -Ccolors.cpt \
    -Bg2f0.2a4+l"Color scale 'jet': dark to light blue, white, yellow and
    red [C=RGB], -T-18/18]" \
    -I0.2 -By+lm -O -K >> $ps
gmt psbasemap -R -J -Tmg26/3.6+w3.0c+d1.63+t45/10/5+ithin,lightgoldenrod+p0
    .1p,gold+l+jCM -O -K >> $ps
gmt psbasemap -R -J -Lx14.5c/-2.3c+c50+w300k+l"Mercator projection. Scale (
    km)"+f \
    -UBL/-0p/-70p -O -K >> $ps
gmt pscoast -R -J -P -Ia/thinnest,blue -Na -N1/thick,white -Wthick,
    darkslategray -Df -O -K >> $ps
gmt logo -Dx7.0/-3.1+o0.1i/0.1i+w2c -O -K >> $ps
gmt pstext -R0/10/0/15 -JX10/10 -X0.1c -Y4.5c -N -O \
    -F+f10p,25,black+jLB >> $ps << EOF
3.0 10.4 Earth geoid image EGM2008 vertical datum 2.5 min resolution
EOF
gmt psconvert Geoid_CF.ps -A1.0c -E720 -Tj -Z
```

Appendix A.3

Listing A3. GMT script for mapping the IGPP Earth Free-Air Anomaly on CAR.

```
#!/bin/bash
gmt img2grd grav_27.1.img -R14/28/2/11.5 -Ggrav_CF.grd -T1 -I1 -E -S0.1 -V
gdalinfo grav_CF.grd -stats
gmt makecpt -Chaxby.cpt -T-85/80 > colors.cpt
ps=Grav_CF.ps
gmt grdimage grav_CF.grd -Ccolors.cpt -R14/28/2/11.5 -JM6.0i -P -I+a15+ne0
    .75 -Xc -K > $ps
gmt grdcontour grav_CF.grd -R -J -C20 -A40 -Wthinner -O -K >> $ps
gmt psbasemap -R -J --MAP_FRAME_AXES=WEsN \
    --FORMAT_GEO_MAP=ddd:mm:ssF \
    -Bpx4f2a2 -Bpyg4f2a2 -Bsxg2 -Bsyg2 \
    -B+t"Free-air gravity anomaly on Central African Republic" -O -K >> $ps
gmt psscale -Dg14/1+w15.0c/0.15i+h+o0.3/0i+ml+e -R -J -Ccolors.cpt \
    -Bg20f1a10+l"Color scale 'haxby' Bill Haxby's color scheme for geoid &
    gravity [C=RGB] -T-200/200]" \
    -I0.2 -By+l"mGal" -O -K >> $ps
gmt psbasemap -R -J -Tdg15/10.5+w1.5c+f3+l -Lx13.5c/-2.3c+c50+w300k+l"
    Mercator projection. Scale: km"+f \
    -UBL/-0p/-70p -O -K >> $ps
gmt pscoast -R -J -P -Ia/thinnest,blue -Na -N1/thickest,deeppink1 -Wthin,
    darkslategray -Df -O -K >> $ps
gmt logo -Dx7.0/-3.1+o0.1i/0.1i+w2c -O -K >> $ps
gmt pstext -R0/10/0/15 -JX10/10 -X0.5c -Y5.0c -N -O \
    -F+f10p,25,black+jLB >> $ps << EOF
2.3 9.2 IGPP Global Earth Free-Air Anomaly, 0.025 mGal resolution
EOF
gmt psconvert Grav_CF.ps -A0.5c -E720 -Tj -Z
```

Appendix A.4

Listing A4. GMT script for estimating the coherency between geophysical grids on CAR.

```
#!/bin/bash
# Extract subsets of img/grd files in geographic format ----------------->
gmt grdcut GEBCO_2019.nc -R14/28/2/11.5 -Gcf_relief.nc
gmt grdconvert n00e00/w001001.adf geoid_CF.grd
gmt img2grd grav_27.1.img -R14/28/2/11.5 -Ggrav_CF.grd -T1 -I1 -E -S0.1 -V
gmt img2grd curv_27.1.img -R14/28/2/11.5 -Ggravvert_CF.grd -T1 -I1 -E -S0.1
     -V
gmt grdcut EMAG2_V2.grd -R14/28/2/11.5 -Gcf_mag.nc
gmt grdcut @earth_wdmam_03m -R14/28/2/11.5 -Gcf_mag_wdmam.nc
gmt grdfft cf_mag_wdmam.nc cf_relief.nc -E+wk+n -Na+d+wtmp > cross_spectra1
    .txt
gmt set FONT_TITLE 12p GMT_FFT kiss
# make cpt for rasters ----------------->
gmt makecpt -Cturbo -T212/1820 > z.cpt # topo
gmt makecpt -Crainbow -T-18/18 > g.cpt # geoid
gmt makecpt -Cjet.cpt -T-40/40 > c.cpt # grav
gmt makecpt -Chaxby.cpt -T-85/80 > d.cpt # vert grav
gmt makecpt -Cwysiwyg.cpt -T-1000/512 > m.cpt # EMAG2
gmt makecpt -Cmag -T-933/375 > n.cpt # WDMAM
ps=Coherency_CF.ps
# map 1 lower left ----------------->
gmt grdimage cf_relief.nc -R14/28/2/11.5 \
    -I+a0+nt1 -JM6.0c -Cz.cpt -P -K -X1.474i -Y1i > $ps
gmt psbasemap -R14/28/2/11.5 -JM6.0c \
    -Ba -BWSne+t"IGPP Global Earth Relief"  -UBL/-5p/-40p \
    --MAP_TITLE_OFFSET=0.1c -O -K >> $ps
# map 2 lower right ----------------->
gmt grdimage geoid_CF.grd -R14/28/2/11.5 \
    -I+a0+nt1 -JM6.0c -Cg.cpt -O -K -X7.5c >> $ps
gmt psbasemap -R14/28/2/11.5 -JM6.0c \
    --MAP_TITLE_OFFSET=0.1c -Ba -BWSne+t"Geoid model EGM2008" -O -K  >> $ps
# map 3 upper left ----------------->
gmt grdimage gravvert_CF.grd -R14/28/2/11.5 -I+a0+nt1 -JM6.0c \
    -Cc.cpt -O -K -X-7.5c -Y6.0c >> $ps
gmt psbasemap -R14/28/2/11.5 -JM6.0c -Ba \
    -BWSne+t"Vertical gravity gradient" \
    --MAP_TITLE_OFFSET=0.1c -O -K >> $ps
# map 4 upper right ----------------->
gmt grdimage grav_CF.grd -R14/28/2/11.5 -I+a0+nt1 -JM6.0c -Cd.cpt -O -K -X7
    .5c >> $ps
gmt psbasemap -R14/28/2/11.5 -JM6.0c -Ba -BWSne+t"Free-air gravity anomaly"
     \
    --MAP_TITLE_OFFSET=0.1c -O -K >> $ps
# map 5 upper left EMAG2 ----------------->
gmt grdimage cf_mag.nc -R14/28/2/11.5 -I+a0+nt1 -JM6.0c \
    -Cm.cpt -O -K -X-7.5c -Y6.0c >> $ps
gmt psbasemap -R14/28/2/11.5 -JM6.0c -Ba -BWSne+t"EMAG2 for CAR" \
    --MAP_TITLE_OFFSET=0.1c -O -K >> $ps
# Bangui magnetic anomaly
gmt psbasemap -R -J -D18/5/22/7r -F+pthickest,white -O -K >> $ps
# map 6 upper right ----------------->
gmt grdimage cf_mag_wdmam.nc -R14/28/2/11.5 -I+a0+nt1 -JM6.0c -Cn.cpt -O -K
     -X7.5c >> $ps
gmt psbasemap -R -J -D18/5/22/7r -F+pthickest,white -O -K >> $ps
gmt psbasemap -R14/28/2/11.5 -JM6.0c -Ba -BWSne+t"WDMAM for CAR" \
    --MAP_TITLE_OFFSET=0.1c -O -K >> $ps
# plot coherency ----------------->
gmt psxy -R3/100/0/1 -JX14.0cl/3.5c -Bx2g3+u"mGal" -Byaf0.04g0.2+l"
    Coherency@+2@+" \
    -BWSnE+t"Coherency between vertical gradient and free-air gravity
    anomaly"+gazure \
    --MAP_GRID_PEN_PRIMARY=thinnest,dimgray \
    --MAP_GRID_PEN_SECONDARY=thinner,dimgray \
    -X-7.5cm -Y6.0c cross_spectra.txt -i0,15 -W0.1p -O -K >> $ps
```

```
gmt psxy -R -J cross_spectra.txt -i0,15,16 -Sc0.15c -Gred -W0.25p -Ey -O -K
    >> $ps
gmt logo -Dx7.5c/-2.0c+o-2.0c/-17.5c+w2c -O >> $ps
# Convert to image file by GhostScript
gmt psconvert Coherency_CF.ps -A1.0c -E720 -Tj -Z
# Unix remove files
rm -f cross.txt *_tmp.nc ?.cpt bbox
```

References

1. Ndam Njikam, M.M.; Meying, A.; Zanga Amougou, A.; Ngon Ngon, G.F. Mapping transpressional and transtensional relay zones by coupling geological and geophysical field data: The case of the central Cameroon shear zone in the Mbere administrative division of the Adamawa region in Cameroon. *J. Afr. Earth Sci.* **2023**, *199*, 104816. [CrossRef]
2. Amponsah, T.Y.; Danuor, S.K.; Wemegah, D.D.; Forson, E.D. Groundwater potential characterisation over the Voltaian basin using geophysical, geological, hydrological and topographical datasets. *J. Afr. Earth Sci.* **2022**, *192*, 104558. [CrossRef]
3. Lemenkova, P.; Debeir, O. Recognizing the Wadi Fluvial Structure and Stream Network in the Qena Bend of the Nile River, Egypt, on Landsat 8–9 OLI Images. *Information* **2023**, *14*, 249. [CrossRef]
4. Lemenkova, P.; Debeir, O. Computing Vegetation Indices from the Satellite Images Using GRASS GIS Scripts for Monitoring Mangrove Forests in the Coastal Landscapes of Niger Delta, Nigeria. *J. Mar. Sci. Eng.* **2023**, *11*, 871. [CrossRef]
5. Matende, K.N.; Ranganai, R.T.; Mickus, K.L.; Lelièvre, P.G.; Mapeo, R.B.; Ramotoroko, C.D. Geophysical and geological investigation of the spatial and subsurface extent of the Segwagwa and Masoke igneous ring complexes in southeast Botswana: Geotectonic implications. *J. Afr. Earth Sci.* **2023**, *197*, 104766. [CrossRef]
6. Steuer, A.; Smirnova, M.; Becken, M.; Schiffler, M.; Günther, T.; Rochlitz, R.; Yogeshwar, P.; Mörbe, W.; Siemon, B.; Costabel, S.; et al. Comparison of novel semi-airborne electromagnetic data with multi-scale geophysical, petrophysical and geological data from Schleiz, Germany. *J. Appl. Geophys.* **2020**, *182*, 104172. [CrossRef]
7. Calamita, G.; Gallipoli, M.; Gueguen, E.; Sinisi, R.; Summa, V.; Vignola, L.; Stabile, T.; Bellanova, J.; Piscitelli, S.; Perrone, A. Integrated geophysical and geological surveys reveal new details of the large Montescaglioso (southern Italy) landslide of December 2013. *Eng. Geol.* **2023**, *313*, 106984. [CrossRef]
8. Di Maio, R.; De Paola, C.; Forte, G.; Piegari, E.; Pirone, M.; Santo, A.; Urciuoli, G. An integrated geological, geotechnical and geophysical approach to identify predisposing factors for flowslide occurrence. *Eng. Geol.* **2020**, *267*, 105473. [CrossRef]
9. Lar, U.A.; Bata, T.; Dibal, H.; Yusuf, S.N.; Lekmang, I.; Goyit, M.; Yenne, E. Potential petroleum prospects in the middle Benue trough, central Nigeria: Inferences from integrated applications of geological, geophysical and geochemical studies. *Sci. Afr.* **2023**, *19*, e01436. [CrossRef]
10. Ngene, T.; Mukhopadhyay, M.; Ampana, S. Reconnaissance investigation of geothermal resources in parts of the Middle Benue Trough, Nigeria using remote sensing and geophysical methods. *Energy Geosci.* **2022**, *3*, 360–371. [CrossRef]
11. Cheng, H.; Huang, Y.; Zhang, W.; Xu, Q. Physical process-based runout modeling and hazard assessment of catastrophic debris flow using SPH incorporated with ArcGIS: A case study of the Hongchun gully. *CATENA* **2022**, *212*, 106052. [CrossRef]
12. Konwea, C.I.; Evurani, D.E.; Ajayi, O. Assessment of groundwater potential of the Obafemi Awolowo University Estate, Southwestern Nigeria. *Sci. Afr.* **2023**, *20*, e01597. [CrossRef]
13. Al-Khersan, E.H.; Ali, S.M.; Al-Yasi, A.I. Environmental geophysical study for ideal locations of landfill within Iraqi Southern Desert. *J. Appl. Geophys.* **2022**, *204*, 104678. [CrossRef]
14. Saha, A.; Nath, A.; Dey, A.K. Multivariate geophysical index-based prediction of the compression index of fine-grained soil through nonlinear regression. *J. Appl. Geophys.* **2022**, *204*, 104706. [CrossRef]
15. Apeh, O.I.; Tenzer, R. Development of tailored gravity model based on global gravitational and topographic models and terrestrial gravity data for geophysical exploration of southern benue trough in southeast Nigeria. *J. Appl. Geophys.* **2022**, *198*, 104561. [CrossRef]
16. Shebl, A.; Abdelaziz, M.I.; Ghazala, H.; Araffa, S.A.S.; Abdellatif, M.; Csámer, Á. Multi-criteria ground water potentiality mapping utilizing remote sensing and geophysical data: A case study within Sinai Peninsula, Egypt. *Egypt. J. Remote Sens. Space Sci.* **2022**, *25*, 765–778. [CrossRef]
17. Jones, A.G.; Afonso, J.C.; Fullea, J. Geochemical and geophysical constrains on the dynamic topography of the Southern African Plateau. *Geochem. Geophys. Geosyst.* **2017**, *18*, 3556–3575. [CrossRef]
18. Gorman, G.; Piggott, M.; Wells, M.; Pain, C.; Allison, P. A systematic approach to unstructured mesh generation for ocean modelling using GMT and Terreno. *Comput. Geosci.* **2008**, *34*, 1721–1731. [CrossRef]
19. Sobh, M.; Ebbing, J.; Mansi, A.H.; Götze, H.J.; Emry, E.L.; Abdelsalam, M.G. The Lithospheric Structure of the Saharan Metacraton From 3-D Integrated Geophysical-Petrological Modeling. *J. Geophys. Res. Solid Earth* **2020**, *125*, e2019JB018747. [CrossRef]
20. Lemenkova, P.; Debeir, O. Quantitative Morphometric 3D Terrain Analysis of Japan Using Scripts of GMT and R. *Land* **2023**, *12*, 261. [CrossRef]
21. Girdler, R.; Taylor, P.; Frawley, J. A possible impact origin for the Bangui magnetic anomaly (Central Africa). *Tectonophysics* **1992**, *212*, 45–58. [CrossRef]

22. Baticle, Y. Impact du développement de Bangui (R.C.A.) sur le paysage périurbain (Suburban landscape of Bangui (R.C.A.): The impact of urban growth). *Bull. l'Assoc. Géogr. Fr.* **1994**, *71*, 152–155. . [CrossRef]
23. Villien, F.; Pirovano, J.P.; Soumille, P.; Vidal, P. Bangui, capitale d'un pays enclavé d'Afrique centrale. Étude historique et géographique. *Pays Enclavés* **1990**, *4*, 1–202.
24. Vennetier, P. La navigation intérieure en Afrique noire: Le réseau français Congo-Oubangui. *Cah. d'Outre-Mer* **1959**, *12*, 321–348. [CrossRef]
25. Regan, R.D.; Marsh, B.D. The Bangui Magnetic Anomaly: Its geological origin. *J. Geophys. Res. Solid Earth* **1982**, *87*, 1107–1120. [CrossRef]
26. Ouabego, M.; Quesnel, Y.; Rochette, P.; Demory, F.; Fozing, E.; Njanko, T.; Hippolyte, J.C.; Affaton, P. Rock magnetic investigation of possible sources of the Bangui magnetic anomaly. *Phys. Earth Planet. Inter.* **2013**, *224*, 11–20. [CrossRef]
27. Njiteu Tchoukeu, C.D.; Basseka, C.A.; Djomani, Y.P.; Rousse, S.; Etame, J.; Llubes, M.; Seoane, L.; Som Mbang, C.; Eyike Yomba, A. Crustal thickness, depth to the bottom of magnetic sources and thermal structure of the crust from Cameroon to Central African Republic: Preliminary results for a better understanding of the origin of the Bangui Magnetic Anomaly. *J. Afr. Earth Sci.* **2021**, *179*, 104206. [CrossRef]
28. Kochemasov, G.G.; Chuprov, A.I. The Bangui Magnetic Anomaly in Central Africa in the Light of New Geological Evidence. *Int. Geol. Rev.* **1990**, *32*, 151–161. [CrossRef]
29. Njiteu Tchoukeu, C.D.; Sobh, M.; Basseka, C.A.; Mouzong, M.; Djomani, Y.P.; Etame, J. The mechanical behaviour of the lithosphere beneath the Chad Basin and the Bangui Magnetic Anomaly. Insights from Moho depth and effective elastic thickness estimates. *J. Afr. Earth Sci.* **2021**, *182*, 104299. [CrossRef]
30. Felix Toteu, S. IGCP 470: The Neoproterozoic Pan-African Belt of Central-Africa: Sedimentation, Deformation History Magmatism, Metamorphism and Geotectonic Evolution. *Gondwana Res.* **2002**, *5*, 906–907. [CrossRef]
31. Ravat, D.; Hinze, W.; von Frese, R. Analysis of MAGSAT magnetic contrasts across Africa and South America. *Tectonophysics* **1992**, *212*, 59–76. . [CrossRef]
32. Arkani-Hamed, J.; Strangway, D. An interpretation of magnetic signatures of aulacogens and cratons in Africa and South America. *Tectonophysics* **1985**, *113*, 257–269. [CrossRef]
33. Wilson, M.; Guiraud, R. Magmatism and rifting in Western and Central Africa, from Late Jurassic to Recent times. *Tectonophysics* **1992**, *213*, 203–225. . [CrossRef]
34. Toteu, S.F.; de Wit, M.; Penaye, J.; Drost, K.; Tait, J.A.; Bouyo, M.H.; Van Schmus, W.R.; Jelsma, H.; Moloto-A-Kenguemba, G.R.; da Silva Filho, A.F.; et al. Geochronology and correlations in the Central African Fold Belt along the northern edge of the Congo Craton: New insights from U-Pb dating of zircons from Cameroon, Central African Republic, and south-western Chad. *Gondwana Res.* **2022**, *107*, 296–324. [CrossRef]
35. Genik, G. Regional framework, structural and petroleum aspects of rift basins in Niger, Chad and the Central African Republic (C.A.R.). *Tectonophysics* **1992**, *213*, 169–185. . [CrossRef]
36. Vervelidou, F.; Lesur, V. Unveiling Earth's Hidden Magnetization. *Geophys. Res. Lett.* **2018**, *45*, 12283–12292. [CrossRef]
37. Poidevin, J.L. Les Ceintures de Roches Vertes de la Republique Centrafricaine (Bandas, Boufoyo, Bogoin, Mbomou). Contribution a la Connaissance du Precambrien du Nord du Craton du Congo. PhD Thesis, Université Clermont-Ferrand II, Clermont-Ferrand, France, 1991.
38. Boulvert, Y. *Esquisse de l'Histoire Géologique de la RCA*; Institut Français de Recherche Scientifique pour le Développement en Coopération, ORSTOM: Bangui, Central African Republic, 1983.
39. Poidevin, J.; Dostal, J.; Dupuy, C. Archaean greenstone belt from the Central African Republic (Equatorial Africa). *Precambrian Res.* **1981**, *16*, 157–170. [CrossRef]
40. Dostal, J.; Dupuy, C.; Poidevin, J.L. Geochemistry of Precambrian basaltic rocks from the Central African Republic (Equatorial Africa). *Can. J. Earth Sci.* **1985**, *22*, 653–662. [CrossRef]
41. Poidevin, J.L. Le protérozoïque supérieur de la République centrafricaine. *Geol. Wetcnschappen* **1985**, *8*, 1–75.
42. Poidevin, J.L. Boninite-like rocks from the Palaeoproterozoic greenstone belt of Bogoin, Central African Republic: Geochemistry and petrogenesis. *Precambrian Res.* **1994**, *68*, 97–113. [CrossRef]
43. Cornacchia, M.; Giorgi, L.; Caruba, C.; Vivier, G. Existence d'une zone de suture sur la marge nord du craton congolais (secteur de Bangui, centre ouest de la République Centrafricaine). *C. R. l'Acad. Sci. Sér. 2 Méc. Phys. Chim. Sci. l'Univ. Sci. Terre* **1989**, *308*, 107–110.
44. Tanko, E.; Danguene, P.; Tsoungui, P.; Ganno, S.; Wambo, J.D.T.; Tchoupe, B.G.T.; Nono, G.D.K.; Ngnotue, T.; Kankeu, B.; Biandja, J.; et al. Geochemistry and zircon U–Pb ages of the Paleoproterozoic ultramafic rocks of the Mbi Valley, Boali area, Central African Republic. *Acta Geochim.* **2022**, *41*, 515–535. [CrossRef]
45. Danguene, P.; Ngnotue, T.; Ganno, S.; Biandja, J.; Kankeu, B.; Nzenti, J. Paleoproterozoic Synkinematic Magnesian High-K Magmatism from the Tamkoro-Bossangoa Massif, along the Bossangoa-Bossembele Shear Zone in North-Western Central African Republic. *J. Geosci. Geomat.* **2014**, *2*, 151–164. [CrossRef]
46. Poidevin, J.; Pin, C. 2 Ga U-Pb zircon dating of Mbi granodiorite (Central African Republic) and its bearing on the chronology of the Proterozoic of Central Africa. *J. Afr. Earth Sci. (1983)* **1986**, *5*, 581–587. [CrossRef]

47. Tanko Njiosseu, E.; Danguene, P.E.; Ngnotue, T.; Ganno, S.; Nono, G.D.K.; Nlend, C.D.N.; Kankeu, B.; Biandja, J.; Nzenti, J.P. Petrology and geochronology of metamorphic rocks from the Bossangoa-Bossembélé area, Northern Central African Republic—Evidence for Palaeoproterozoic high-grade metamorphism in the North Equatorial Fold Belt. *Arab. J. Geosci.* **2021**, *14*, 1660. [CrossRef]
48. Gérard, G.; Gérard, J. Carte Géologique de Reconnaissance de l'A.E.F. Notice Explicative sur la Feuille Berbérati-Est—Scale: 500,000—Sheet Number/Numéro de Feuille/Bladnummer: NB 33 SE-E 33 Direction des Mines et de la Géologie de l'A.E.F-Brazaville. 1953. Available online: https://geocatalogue.africamuseum.be/geonetwork/srv/api/records/BE-RMCA-EARTHS-018894 (accessed on 7 April 2023).
49. Toyama, R.; Ngos, S.; Sababa, E.; Tchouatcha, M.S.; Danguene Yedidya, E.P.; Préat, A.; Ndjigui, P.D. Paleoenvironment reconstruction of the Proterozoic carbonate platform, Ombella-M'poko formation (Central African Republic). *J. Afr. Earth Sci.* **2019**, *156*, 108–117. [CrossRef]
50. Censier, C.; Lang, J. Sedimentary processes in the Carnot Formation (Central African Republic) related to the palaeogeographic framework of Central Africa. *Sediment. Geol.* **1999**, *127*, 47–64. [CrossRef]
51. Censier, C. Characteristics of Mesozoic fluvio-lacustrine formations of the western Central African Republic (Carnot Sandstones) by means of mineralogical and exoscopic analyses of detrital material. *J. Afr. Earth Sci.* **1990**, *10*, 385–398. [CrossRef]
52. Loule, J.P.; Pospisil, L. Geophysical evidence of Cretaceous volcanics in Logone Birni Basin (Northern Cameroon), Central Africa, and consequences for the West and Central African Rift System. *Tectonophysics* **2013**, *583*, 88–100. [CrossRef]
53. Lavreau, J.; Poidevin, J.; Ledent, D.; Liegeois, J.; Weis, D. Contribution to the geochronology of the basement of the Central African Republic. *J. Afr. Earth Sci.* **1990**, *11*, 69–82. [CrossRef]
54. Cornacchia, M.; Giorgi, L. Discordances majeures et magmatismes des séries précambriennes de la région de Bogoin (Centre ouest de la République Centrafricaine). *J. Afr. Earth Sci.* **1989**, *9*, 221–226. [CrossRef]
55. Topien, R.M.; Moloto-A-Kenguemba, G.; Traore, M.; Rajendran, S.; Kouassi, B.R. Litho-structural mapping and structural evolution of the Bocaranga pluton, northwest Adamawa-Yadé domain, Central African Republic. *J. Afr. Earth Sci.* **2023**, *198*, 104793. [CrossRef]
56. Mestraud, J.L.; Bouvier, P.; Dongala, M.; Touveron, G. *Carte Géologique de la Républiquc Centrafricaine à l'Échelle du 1:1,500,000*; Bureau de Recherches Géologiques et Minières (BRGM): Paris, France, 1964.
57. Vonto, D.C.; Tchakounte, N.J.; Gentry, F.C.; Zaguy-Guerembo, R.L.; Zame, P.Z.; Djanarthany, S.; Nkoumbou, C. Geology and geotechnical characteristics of the Gbago and Ngouaka plutonic rocks, North East of Bangui, Central Africa Republic. *J. Afr. Earth Sci.* **2020**, *167*, 103831. [CrossRef]
58. Boulvert, Y. *Étude Géomorphologique de la République Centrafricaine Carte à 1/1,000,000 en Deux Feuilles Ouest et Est*; ORSTOM Éditions: Paris, France, 1995; Volume 110.
59. Censier, C.; Michel, J.; Lamouille, B. *Rapport Final du Projet d'Appui au Secteur Artisanal du Diamant en République Centrafricaine (PASAD) [01/09/96–31/08/98]*; Technical Report 655, République Centrafricaine Ministère de la Réforme Economique du Plan et de la Coopération Internationale; BRGM Service Minier National, Département de l'Exploration: Orleans, France, 1998.
60. Censier, C.; Tourenq, J. Crystal forms and surface textures of alluvial diamonds from the Western Region of the Central African Republic. *Miner. Depos.* **1995**, *30*, 314–322. [CrossRef]
61. Malpeli, K.C.; Chirico, P.G. A sub-national scale geospatial analysis of diamond deposit lootability: The case of the Central African Republic. *Extr. Ind. Soc.* **2014**, *1*, 249–259. [CrossRef]
62. Berthoumieux, G.; Delany, F. Mission diamant dans l'Ouest-Oubangui. *Bull. Serv. Mines Géol.* **1957**, 77–91.
63. Kpeou, J.; Béziat, D.; Salvi, S.; Estrade, G.; Moloto-A-Kenguemba, G.; Debat, P. Gold mineralization related to Proterozoic cover in the Congo craton (Central African Republic): A consequence of Panafrican events. *J. Afr. Earth Sci.* **2020**, *166*, 103825. [CrossRef]
64. Chirico, P.G.; Barthélémy, F.; Ngbokoto, F.A. *Les Ressources Potentielles en Diamants Alluviaux et l'Évaluation de la Capacité de Production en République Centrafricaine*; Technical Report 2010-5043; U.S. Geological Survey: Reston, VA, USA, 2013; 23p.
65. Chirico, P.G.; Barthélémy, F.; Ngbokoto, F.A. *Alluvial Diamond Resource Potential and Production Capacity Assessment of the Central African Republic*; Technical Report 2010-5043; U.S. Geological Survey: Reston, VA, USA, 2007.
66. Nguimalet, C.R.; Orange, D.; Waterendji, J.P.; Yambele, A. Hydroclimatic Dynamics of Upstream Ubangi River at Mobaye, Central African Republic. In *Congo Basin Hydrology, Climate, and Biogeochemistry*; American Geophysical Union (AGU): Washington, DC, USA, 2022; Chapter 6, pp. 83–96. [CrossRef]
67. Suchel, J.B. L'exploitation forestière en République Centrafricaine. *Cah. d'Outre-Mer* **1968**, *21*, 324–330. [CrossRef]
68. Spinage, C.A. First steps in the ecology of the Bamingui-Bangoran National Park, Central African Republic. *Afr. J. Ecol.* **1988**, *26*, 73–88. [CrossRef]
69. Villien, F. L'agriculture dans la ville: L'exemple de Bangui. *Cah. d'Outre-Mer* **1988**, *41*, 283–302. . [CrossRef]
70. Quantin, P. *Les Sols de la République Centrafricaine*; Technical Report 16; Mérn. Office de la Recherche Scientifique et Technique Outre-Mer (ORSTOM): Paris, France, 1965; 113p.
71. Prioul, C. Les cultures maraîchères à Bangui. *Cah. d'Outre-Mer* **1969**, *22*, 191–202. [CrossRef]
72. Combeau, A.; Quantin, P. Observation sur Ies relations entre stabilité structurale et matiére organique dans quelques sols d'Afrique Centrale. *Cah. Off. Rech. Sci. Tech. Outre-Mer (ORSTOM) Pédolog.* **1964**, *2*, 3–11.
73. Quantin, P. *Reconnaissance Pédologique au Nord-Est de la République Centrafricaine (Birao)*; Technical Report Rapport de Terrain; Office de la Recherche Scientifique et Technique Outre-Mer (ORSTOM) Inédit: Paris, France, 1962; p. 38.

74. Salomon, J.N.; Boulvert, Y. Sur l'existence de paléo-crypto karsts dans le bassin de l'Oubangui (République centrafricaine). *Karstologia* **1988**, *11*, 37–48. [CrossRef]
75. GEBCO Compilation Group. *GEBCO_2022 Grid—A Continuous Terrain Model of the Global Oceans and Land*; British Oceanographic Data Centre (BODC): Liverpool, UK, 2022. [CrossRef]
76. NASA JPL. *NASA Shuttle Radar Topography Mission Global 3 Arc Second*; NASA EOSDIS Land Processes DAAC, Data Set; NASA: Washington, DC, USA, 2013. [CrossRef]
77. NOAA National Geophysical Data Center. *ETOPO1 1 Arc-Minute Global Relief Model*; NOAA National Centers for Environmental Information: Asheville, NC, USA, 2009.
78. Sandwell, D.T.; Harper, H.; Tozer, B.; Smith, W.H. Gravity field recovery from geodetic altimeter missions. *Adv. Space Res.* **2021**, *68*, 1059–1072. [CrossRef]
79. Pavlis, N.K.; Holmes, S.A.; Kenyon, S.C.; Factor, J.K. The development and evaluation of the Earth Gravitational Model 2008 (EGM2008). *J. Geophys. Res. Solid Earth* **2012**, *117*, B04406. [CrossRef]
80. QGIS Development Team. *QGIS Geographic Information System*; Open Source Geospatial Foundation: Chicago, IL, USA, 2009.
81. Traore, M.; Takodjou Wambo, J.D.; Ndepete, C.P.; Tekin, S.; Pour, A.B.; Muslim, A.M. Lithological and alteration mineral mapping for alluvial gold exploration in the south east of Birao area, Central African Republic using Landsat-8 Operational Land Imager (OLI) data. *J. Afr. Earth Sci.* **2020**, *170*, 103933. [CrossRef]
82. Runge, J.; Nguimalet, C.R. Physiogeographic features of the Oubangui catchment and environmental trends reflected in discharge and floods at Bangui 1911–1999, Central African Republic. *Geomorphology* **2005**, *70*, 311–324. [CrossRef]
83. Traore, M.; Lee, M.S.; Rasul, A.; Balew, A. Assessment of land use/land cover changes and their impacts on land surface temperature in Bangui (the capital of Central African Republic). *Environ. Chall.* **2021**, *4*, 100114. [CrossRef]
84. Spinellis, D. Drawing Tools. *IEEE Softw.* **2009**, *26*, 12–13. [CrossRef]
85. Lemenkova, P.; Debeir, O. Satellite Altimetry and Gravimetry Data for Mapping Marine Geodetic and Geophysical Setting of the Seychelles and the Somali Sea, Indian Ocean. *J. Appl. Eng. Sci.* **2022**, *12*, 191–202. [CrossRef]
86. Kasalica, V.; Lamprecht, A.L. Automated composition of scientific workflows: A case study on geographic data manipulation. In Proceedings of the 2018 IEEE 14th International Conference on e-Science (e-Science), Amsterdam, The Netherlands, 29 October–1 November 2018; pp. 362–363. [CrossRef]
87. Lemenkova, P.; Debeir, O. Seismotectonics of Shallow-Focus Earthquakes in Venezuela with Links to Gravity Anomalies and Geologic Heterogeneity Mapped by a GMT Scripting Language. *Sustainability* **2022**, *14*, 15966. [CrossRef]
88. Yadav, A.; Saraswat, S.; Faujdar, N. Geological Information Extraction from Satellite Imagery Using Machine Learning. In Proceedings of the 2022 10th International Conference on Reliability, Infocom Technologies and Optimization (Trends and Future Directions) (ICRITO), Noida, India, 13–14 October 2022; pp. 1–5. [CrossRef]
89. Lemenkova, P.; Debeir, O. R Libraries for Remote Sensing Data Classification by k-means Clustering and NDVI Computation in Congo River Basin, DRC. *Appl. Sci.* **2022**, *12*, 12554. [CrossRef]
90. Senturk, S.; Cakir, Z.; Berk Ustundag, B. The potential of Sentinel-IA interferometric SAR data in monitoring of surface subsidence caused by overdrafting groundwater in agricultural areas. In Proceedings of the 2016 Fifth International Conference on Agro-Geoinformatics (Agro-Geoinformatics), Tianjin, China, 18–20 July 2016; pp. 1–4. [CrossRef]
91. Lemenkova, P.; Debeir, O. Satellite Image Processing by Python and R Using Landsat 9 OLI/TIRS and SRTM DEM Data on Côte d'Ivoire, West Africa. *J. Imaging* **2022**, *8*, 317. [CrossRef] [PubMed]
92. Wessel, P.; Smith, W.H.F. Free software helps map and display data. *EOS Trans. Am. Geophys. Union* **1991**, *72*, 441–446. [CrossRef]
93. Wessel, P.; Luis, J.F.; Uieda, L.; Scharroo, R.; Wobbe, F.; Smith, W.H.F.; Tian, D. The Generic Mapping Tools Version 6. *Geochem. Geophys. Geosyst.* **2019**, *20*, 5556–5564. [CrossRef]
94. Le Stunff, Y.; Ricard, Y. Topography and geoid due to lithospheric mass anomalies. *Geophys. J. Int.* **1995**, *122*, 982–990. [CrossRef]
95. Hager, B.H. Global isostatic geoid anomalies for plate and boundary layer models of the lithosphere. *Earth Planet. Sci. Lett.* **1983**, *63*, 97–109. [CrossRef]
96. Hager, B.H.; Clayton, R.W. Constraints on the Structure of Mantle Convection Using Seismic Observations, Flow Models, and the Geoid. In *Mantle Convection: Plate Tectonics and Global Dynamics*; Chapter Fluid Mechanics of Astrophysics and Geophysics; Gordon and Breach Science Publishers: New York, NY, USA, 1989; Volume 4, pp. 657–763.
97. Richards, F.D.; Hoggard, M.J.; Ghelichkhan, S.; Koelemeijer, P.; Lau, H.C. Geodynamic, geodetic, and seismic constraints favour deflated and dense-cored LLVPs. *Earth Planet. Sci. Lett.* **2023**, *602*, 117964. [CrossRef]
98. Dorbath, C.; Dorbath, L.; Gaulon, R.; Hatzfeld, D. Seismological investigation of the Bangui magnetic anomaly region and its relation to the margin of the Congo craton. *Earth Planet. Sci. Lett.* **1985**, *75*, 231–244. . [CrossRef]
99. Moloto-A-Kenguemba, G.R.; Trindade, R.I.; Monié, P.; Nédélec, A.; Siqueira, R. A late Neoproterozoic paleomagnetic pole for the Congo craton: Tectonic setting, paleomagnetism and geochronology of the Nola dike swarm (Central African Republic). *Precambrian Res.* **2008**, *164*, 214–226. [CrossRef]
100. Goussi Ngalamo, J.F.; Sobh, M.; Bisso, D.; Abdelsalam, M.G.; Atekwana, E.; Ekodeck, G.E. Lithospheric structure beneath the Central Africa Orogenic Belt in Cameroon from the analysis of satellite gravity and passive seismic data. *Tectonophysics* **2018**, *745*, 326–337. [CrossRef]
101. Boukeke, D.B. Structures Crustales d'Afrique Centrale Déduites des Anomalies Graviiviétriques et Magnétiques: Le Domaine Précambrien de la République Centrafricaine et du Sud Cameroun. Ph.D. Thesis, L'Université Paris-Sud, Paris, France, 1994.

102. Daly, M.C.; Green, P.; Watts, A.B.; Davies, O.; Chibesakunda, F.; Walker, R. Tectonics and Landscape of the Central African Plateau and their Implications for a Propagating Southwestern Rift in Africa. *Geochem. Geophys. Geosyst.* **2020**, *21*, e2019GC008746. [CrossRef]
103. Albouy, Y.; Godivier, R. *Cartes Gravimétriques de la République Centrafricaine*; ORSTOM: Paris, France, 1981; p. 8.
104. Milesi, J.; Toteu, S.; Deschamps, Y.; Feybesse, J.; Lerouge, C.; Cocherie, A.; Penaye, J.; Tchameni, R.; Moloto-A-Kenguemba, G.; Kampunzu, H.; et al. An overview of the geology and major ore deposits of Central Africa: Explanatory note for the 1:4,000,000 map "Geology and major ore deposits of Central Africa". *J. Afr. Earth Sci.* **2006**, *44*, 571–595. [CrossRef]
105. Chevrot, S. Multichannel analysis of shear wave splitting. *J. Geophys. Res. Solid Earth* **2000**, *105*, 21579–21590. [CrossRef]
106. Forte, A.M.; Peltier, W.R.; Dziewonski, A.M.; Woodward, R.L. Dynamic surface topography: A new interpretation based upon mantle flow models derived from seismic tomography. *Geophys. Res. Lett.* **1993**, *20*, 225–228. [CrossRef]
107. Mapoka, H.; Danguene, Y.; Nzenti, J.; Biandja, J.; Kankeu, B.; Suh, C. Major Structural Features and the Tectonic Evolution of the Bossangoa-Bossembele Basement, Northwestern Central African Republic. *Open Geol. J.* **2011**, *5*, 21–32. [CrossRef]
108. Taylor, P.T. Bangui Anomaly. In *Encyclopedia of Geomagnetism and Paleomagnetism*; Springer: Dordrecht, The Netherlands, 2007; pp. 39–40. [CrossRef]
109. Green, A.G. Interpretation of Project MAGNET Aerornagnetic Profiles Across Africa. *Geophys. J. Int.* **1976**, *44*, 203–228. [CrossRef]
110. Lesur, V.; Hamoudi, M.; Choi, Y.; Dyment, J.; Thébault, E. Building the second version of the World Digital Magnetic Anomaly Map (WDMAM). *Earth Planets Space* **2016**, *68*, 27. [CrossRef]
111. Ravat, D.; Wang, B.; Wildermuth, E.; Taylor, P.T. Gradients in the interpretation of satellite-altitude magnetic data: An example from central Africa. *J. Geodyn.* **2002**, *33*, 131–142. [CrossRef]
112. Zhang, Y.; Gu, Q. Petroleum system of the Fula depression at the Muglad basin in the Central African fault zone. *J. Earth Sci.* **2011**, *22*, 363–370. [CrossRef]
113. de Haro Barbas, B.F.; Elias, A.G.; Cnossen, I.; Zossi de Artigas, M. Long-term changes in solar quiet (Sq) geomagnetic variations related to Earth's magnetic field secular variation. *J. Geophys. Res. Space Phys.* **2013**, *118*, 3712–3718. [CrossRef]
114. Maus, S.; Barckhausen, U.; Berkenbosch, H.; Bournas, N.; Brozena, J.; Childers, V.; Dostaler, F.; Fairhead, J.D.; Finn, C.; von Frese, R.R.B.; et al. EMAG2: A 2-arc min resolution Earth Magnetic Anomaly Grid compiled from satellite, airborne, and marine magnetic measurements. *Geochem. Geophys. Geosyst.* **2009**, *10*, Q08005. [CrossRef]
115. Meyer, B.; Saltus, R.; Chulliat, A. *EMAG2v3: Earth Magnetic Anomaly Grid (2-Arc-Minute Resolution)*, Version 3; NOAA National Centers for Environmental Information: Asheville, NC, USA, 2017. [CrossRef]